J. Fluid Mech. (1997), *vol.* 343, *pp.* 267–301. Printed in the United Kingdom

The influence of friction on the stability of unbounded granular shear flow

By MEHEBOOB ALAM[1] AND PRABHU R. NOTT[2]

[1]Department of Mechanical Engineering, Indian Institute of Science, Bangalore 560012, India
e-mail: alam@mecheng.iisc.ernet.in

[2]Department of Chemical Engineering, Indian Institute of Science, Bangalore 560012, India
e-mail: prnott@chemeng.iisc.ernet.in

(Received 26 August 1996 and in revised form 7 March 1997)

Some recent studies have considered the stability of unbounded rapid granular shear flow, with the sole mechanism for stress generation being instantaneous inelastic collisions between grains. This paper extends these studies by presenting a linear stability analysis in which stress generation due to grain friction is also accounted for. This is accomplished by using the 'frictional–kinetic' model, which integrates in a simple manner the stress arising from the two mechanisms. Solution of the linearized equations of motion is obtained by allowing the wavenumber vector of the disturbances to rotate as a function of time. As in the case of a purely kinetic stress, it is found that the flow is stable to non-layering disturbances. Disturbances in the form of layering modes may lead to instability, depending on the solids fraction and material parameters. Instability is absent altogether if the balance of fluctuational energy is not considered or if the material is assumed to be incompressible. Friction may stabilize or destabilize the flow, depending on the inelasticity of grain collisions and the effective roughness of the medium. When a purely frictional stress is considered, it is found that the system is always neutrally stable. Even if the flow is asymptotically stable, there may be significant transient growth of disturbances due to the non-normality of the associated linear operator. The initial transient growth rate, as well as the temporal maximum of transient growth is enhanced by friction.

1. Introduction

In recent years, the stability of the shear flow of granular materials has received considerable attention (Mello, Diamond & Levine 1991; Savage 1992*b*; Babić 1993; McNamara 1993; Schmid & Kytömaa 1994; Wang, Jackson & Sundaresan 1996). The motivation for the stability analyses arose, at least partly, from the dynamic simulation studies of Hopkins & Louge (1991) and Savage (1992*a*) (see also Goldhirsch, Tan & Zanetti 1993) in which inhomogeneities in the arrangement of particles were observed. Hopkins & Louge (1991) reported persistent clusters of particles during the shearing of an assembly of uniform smooth circular inelastic disks in the absence of gravity. The size and strength of the inhomogeneities in particle distribution were found to depend on the mean volume fraction of particles and the inelasticity of particle collisions. Savage (1992*a*) observed that when an assembly of particles was sheared between rough walls in the absence of gravity, turbulent-like flow occurred in some regions.

Notably, the power spectrum of the fluctuations in the stress had the form of $1/f$ noise. He suggested that these fluctuations were analogous to turbulent fluctuations in fluids. Stress fluctuations of this nature have been observed experimentally by Behringer & Baxter (1991) in the flow of granular materials through a hopper and by Miller, O'Hern & Behringer (1996) in an annular shear cell. The latter have reported the interesting observation that the power spectrum of the stress fluctuations, suitably scaled, is independent of the shear rate.

The appearance of concentration inhomogeneities and fluctuations in the stress has significant bearing on the development of constitutive models for the rheology of granular media, for all available models (understandably) assume uniformity in the distribution of particles and smoothly varying fields. An important question from the point of view of constitutive modelling is whether the observed inhomogeneities and fluctuations can be explained within the continuum framework. If not, constitutive models for granular rheology must incorporate in some manner the inhomogeneous distribution of particles.

Savage (1992b) considered the linear stability of unbounded uniform shear flow to two-dimensional disturbances. Since the velocity in the base state is a function of position, the classical normal mode form with a constant wave vector is not a solution of the linearized disturbance equations. Savage sought a solution of the form first introduced by Thomson (1887), in which the wave vector is allowed to rotate by the mean shear (following Wang *et al.* 1996, we hereafter refer to this form as 'Kelvin modes'). This yields a set of linear differential equations whose coefficients are functions of time. To further simplify the analysis, Savage considered only the initial growth rate of disturbances, which involved obtaining the eigenvalues of the linearized equations with coefficients frozen at $t = 0$. Babić (1993) expanded the analysis of Savage by considering two-dimensional disturbances for an array of disks and three-dimensional disturbances for spheres in uniform shear flow. In general, Savage and Babić observed that at a given density, the initial growth rate was a maximum at some large wavelength; this maximum growth rate increased with the mean density until some intermediate value, beyond which it decreased. Furthermore, the flow tended to be more 'unstable' as the inelasticity of grain collisions increased. Babić also noted that this instability would not be observed in the dynamic simulations with small periodic cells, as they preclude the possibility of unstable disturbances with sufficiently small wavenumber (this is not quite correct, as elaborated in the concluding section of this paper).

The conclusions on the stability of shear flow in the studies of Savage and Babić are based on the initial growth rate of disturbances. However, initial growth of disturbances does not necessarily imply instability, as the growth rates are based on the eigenvalues of the linearized equations with coefficients frozen at $t = 0$, and are therefore relevant only for small t.

More recently, Schmid & Kytömaa (1994) considered the complete differential equations for the disturbances, without freezing the coefficients. They computed the growth function $G(t)$, which is the largest possible amplification at time t over all initial disturbances of unit norm. They observed that for a certain range of the wavenumber vector, $G(t)$ can increase with t and attain a large value. However, for non-zero values of the streamwise wavenumber ($k_x \neq 0$), the individual Fourier modes and the growth function $G(t)$ always decay as $t \to \infty$. They then concluded that the base state of uniform shear is asymptotically stable, but the transient growth of disturbances can trigger instabilities associated with nonlinearities in the governing equations.

All the considerations in the previous two paragraphs were clearly elucidated in the recent paper of Wang *et al.* (1996). More importantly, they pointed out that the conclusion of Schmid & Kytömaa that unbounded uniform shear flow is always linearly stable is incorrect, as they demonstrated the existence of Kelvin modes with $k_x = 0$ which are unstable. Wang *et al.* refer to these as 'layering modes', a definition we have retained in this work. They also noted that the transient growth reported by Schmid & Kytömaa is not a true instability in the sense of Lyapunov, as the initial perturbations may be scaled so that the perturbed state is always within any specified neighbourhood of the base state.

An important point to note is that all the investigations on the stability of granular shear flow referred to above have used one of the kinetic-theory-based models for the rheology, in which particles interact through instantaneous binary collisions. Savage (1992*b*), Babić (1993), Schmid & Kytömaa (1994) and Wang *et al.* (1996) used the model of Lun *et al.* (1984) and McNamara (1993) used the model of Jenkins & Richman (1985). While the physical picture of stress generation from instantaneous collisions between particles is expected to be valid at low densities and high shear rates, the stress arising from frictional forces due to abiding grain contacts will be important at higher densities. The densities for which the frictional stress is significant, and perhaps dominant, can be realized even under gravitational compaction. It is therefore important to extend the analysis of stability of granular shear flow to include the effect of friction.

In this work, we study the linear stability of unbounded uniform shear flow of a granular material in the absence of external body forces to two-dimensional disturbances. We use the 'frictional–kinetic' model of Johnson & Jackson (1987) to describe the stress in the granular medium. This model integrates, in a simple manner, the generation of stress due to particle streaming and collisions and that due to grain friction. We use the critical state model (Jackson 1983; Prakash & Rao 1988) for the frictional contribution to the stress and the model of Lun *et al.* (1984) for the kinetic stress. The linear stability of the base state of uniform shear flow is determined by seeking solutions of the linearized equations in the form of Kelvin modes. We consider asymptotic stability as well as transient behaviour of the linearized operator in the manner of Schmid & Kytömaa (1994) for the complete equations with time-dependent coefficients. We show that unbounded granular shear flow is neutrally stable if the stress is purely frictional. When combined with the kinetic stress, however, friction may stabilize or destabilize the flow when disturbances are in the form of *layering modes* ($k_x = 0$, $k_y \neq 0$), depending on the inelasticity of particle collisions and the roughness of the material; disturbances in the form of *non-layering modes* ($k_x \neq 0$) always decay asymptotically, as in the purely kinetic case. Furthermore, we show that friction has a pronounced effect on the transient growth of disturbances. The maxima in the norms of disturbances are subsequently larger than those corresponding to the purely kinetic case. The disturbance that results in the largest transient growth is found to be the one with $k_x = 0$ and $k_y = 0$.

2. Governing equations

The continuum balances for mass, momentum and fluctuational energy may be written as (Johnson & Jackson 1987)

$$\rho_p \frac{\mathrm{D}v}{\mathrm{D}\tilde{t}} = -\rho_p v(\tilde{\boldsymbol{\nabla}} \cdot \tilde{\boldsymbol{u}}),$$

$$\rho_p v \frac{\mathrm{D}\tilde{\boldsymbol{u}}}{\mathrm{D}\tilde{t}} = \rho_p v \tilde{\boldsymbol{g}} - \tilde{\nabla} \cdot (\tilde{\boldsymbol{\Sigma}}_{\mathrm{k}} + \tilde{\boldsymbol{\Sigma}}_{\mathrm{f}}),$$

$$\tfrac{3}{2}\rho_p v \frac{\mathrm{D}\tilde{T}}{\mathrm{D}\tilde{t}} = -\tilde{\nabla}\tilde{\boldsymbol{q}} - \tilde{\boldsymbol{\Sigma}}_{\mathrm{k}} : \tilde{\nabla}\tilde{\boldsymbol{u}} - \tilde{\mathscr{D}},$$

where v is the particle volume fraction, ρ_p is the intrinsic density of the particles, $\tilde{\boldsymbol{u}}$ is the bulk velocity, $\tilde{\boldsymbol{g}}$ is the acceleration due to gravity and $\tilde{T}$ denotes the grain temperature; $\tilde{\boldsymbol{q}}$ is the flux of fluctuational, or 'pseudo-thermal', energy and $\tilde{\mathscr{D}}$ is the collisional rate of energy dissipation per unit volume. The last of the above equations, which is a balance of fluctuational energy, is required as the transport properties of the granular medium in the kinetic model depend on the grain temperature. The momentum equation reflects the assumption that the total stress in the granular continuum is the sum of collisional–kinetic $\tilde{\boldsymbol{\Sigma}}_{\mathrm{k}}$ (henceforth referred to simply as the kinetic stress) and frictional, $\tilde{\boldsymbol{\Sigma}}_{\mathrm{f}}$, contributions (both defined in the compressive sense), with each calculated independently from constitutive expressions derived for the limits of purely collisional and purely frictional interactions, respectively. Implicit in the derivation of the fluctuational energy balance is the assumption that frictional work generates true thermal energy (heat) and does not contribute to the generation of fluctuational energy (Johnson & Jackson 1987).

Using the particle diameter (d_p) and inverse of the shear rate ($\tilde{\Gamma}^{-1}$) as the natural length and time scales, respectively, the following non-dimensional variables are introduced:

$$(x, y) = \frac{1}{d_p}(\tilde{x}, \tilde{y}), \quad t = \tilde{t}\,\tilde{\Gamma}, \quad (u, v) = \frac{1}{d_p\tilde{\Gamma}}(\tilde{u}, \tilde{v}), \quad T = \frac{\tilde{T}}{d_p^2\tilde{\Gamma}^2},$$

$$\boldsymbol{\Sigma}_{\mathrm{k}} = \frac{\tilde{\boldsymbol{\Sigma}}_{\mathrm{k}}}{\rho_p d_p^2\tilde{\Gamma}^2}, \quad \boldsymbol{\Sigma}_{\mathrm{f}} = \frac{\tilde{\boldsymbol{\Sigma}}_{\mathrm{f}}}{\rho_p d_p^2\tilde{\Gamma}^2}, \quad \boldsymbol{q} = \frac{\tilde{\boldsymbol{q}}}{\rho_p d_p^3\tilde{\Gamma}^3}, \quad \mathscr{D} = \frac{\tilde{\mathscr{D}}}{\rho_p d_p^2\tilde{\Gamma}^3}.$$

The dimensionless balance equations, in the absence of gravity, reduce to the following form:

$$\frac{\mathrm{D}v}{\mathrm{D}t} = -v(\nabla \cdot \boldsymbol{u}), \tag{2.1}$$

$$v\frac{\mathrm{D}\boldsymbol{u}}{\mathrm{D}t} = -\nabla \cdot (\boldsymbol{\Sigma}_{\mathrm{k}} + \boldsymbol{\Sigma}_{\mathrm{f}}), \tag{2.2}$$

$$\tfrac{3}{2}v\frac{\mathrm{D}T}{\mathrm{D}t} = -\nabla\boldsymbol{q} - \boldsymbol{\Sigma}_{\mathrm{k}} : \nabla\boldsymbol{u} - \mathscr{D}. \tag{2.3}$$

2.1. *Constitutive equations for the kinetic model*

We adopt a slightly modified form of the constitutive expressions of Lun *et al.* (1984), as detailed in Johnson & Jackson (1987), for $\boldsymbol{\Sigma}_{\mathrm{k}}$, $\boldsymbol{q}$ and $\mathscr{D}$:

$$\boldsymbol{\Sigma}_{\mathrm{k}} = \left(f_1(v)T - f_3(v)T^{1/2}\nabla \cdot \boldsymbol{u}\right)\boldsymbol{I} - 2f_2(v)T^{1/2}\boldsymbol{S}, \tag{2.4}$$

$$\boldsymbol{q} = -f_4(v)T^{1/2}\nabla T - f_{4h}(v)T^{3/2}\nabla v, \tag{2.5}$$

$$\mathscr{D} = f_5(v)T^{3/2}, \tag{2.6}$$

where

$$\boldsymbol{S} = \tfrac{1}{2}(\nabla\boldsymbol{u} + \nabla\boldsymbol{u}^T) - \tfrac{1}{3}(\nabla \cdot \mathbf{u})\boldsymbol{I},$$

and $\boldsymbol{I}$ is the identity tensor. The non-dimensional functions f_1–f_5 are listed in table 1. These functions depend on the equilibrium radial distribution function $g(v)$, for which

$f_1(\nu)$	$\nu(1+4\eta\nu g(\nu))$
$f_2(\nu)$	$\frac{(2+\alpha)}{3\pi^{1/2}}\left(\frac{5\pi}{96\eta(2-\eta)}\right)\left(1+\frac{8}{5}\eta\nu g(\nu)\right)\left(\frac{1}{g(\nu)}+\frac{8}{5}\eta(3\eta-2)\nu\right)+\frac{8}{5}\eta\nu^2 g(\nu)\Big)$
$f_3(\nu)$	$\frac{8}{3\pi^{1/2}}\eta\nu^2 g(\nu)$
$f_4(\nu)$	$\frac{25\pi^{1/2}}{16\eta(41-33\eta)}\left(1+\frac{12}{5}\eta\nu g(\nu)\right)\left(\frac{1}{g(\nu)}+\frac{12}{5}\eta^2(4\eta-3)\nu\right)+\frac{4}{\pi^{1/2}}\eta\nu^2 g(\nu)$
$f_{4h}(\nu)$	$\frac{25\pi^{1/2}}{16\eta(41-33\eta)}\left(\frac{1}{\nu g(\nu)}+\frac{12}{5}\eta\right)\frac{12}{5}\eta(2\eta-1)(\eta-1)\frac{\mathrm{d}}{\mathrm{d}\nu}(\nu^2 g(\nu))$
$f_5(\nu)$	$\frac{48}{\pi^{1/2}}\eta(1-\eta)\nu^2 g(\nu)$
η	$\frac{1}{2}(1+e_p)$

TABLE 1. Non-dimensional functions

Parameters	Values
$\widetilde{Fr}$	0.05 kg m^{-1} s^{-2}
ν_{min}	0.50
ν_{max}	0.65
$\mathscr{N}$	5
$\mathscr{P}$	2
n	1.03
ϕ	28.5°
ρ_p	2900 kg m^{-3}
d_p	1 mm
α	1.6

TABLE 2. Material properties

we use the form

$$g(\nu) = \frac{1}{1-(\nu/\nu_{max})^{1/3}}. \tag{2.7}$$

This form ensures that $g \to \infty$ when $\nu \to \nu_{max}$ and hence constrains the solids volume fraction to remain less than the maximum-packing value ν_{max}. This form has been used in earlier studies on granular flow (e.g. Johnson & Jackson 1987; Nott & Jackson 1992). The consequence of assuming an alternative form for $g(\nu)$ is discussed in § 6. The parameter α appearing in the expression for $f_2(\nu)$ reflects the anisotropy of the pair distribution function – its value is given in table 2.

2.2. *Constitutive equations for the frictional stresses*

Constitutive theories for the frictional stress are empirical in nature and do not depend on quantities directly related to physical characteristics of the grains such as the particle size, or surface roughness. In this work, we use the critical state model for the frictional stress. We give only a brief description of its features and refer to Jackson (1983) for a detailed description of the physical basis of the theory. The model is described for two-dimensional flow, as that is the concern of this study.

The model is conveniently described in terms of the Sokolovski stress variables σ, τ, and γ, defined as

$$\sigma = \tfrac{1}{2}(\sigma_1+\sigma_2), \quad \tau = \tfrac{1}{2}(\sigma_1-\sigma_2),$$

where σ_1 and σ_2 are the major and minor principal frictional stresses, respectively, and γ is the angle between the x-axis and the direction of σ_1, measured in the clockwise

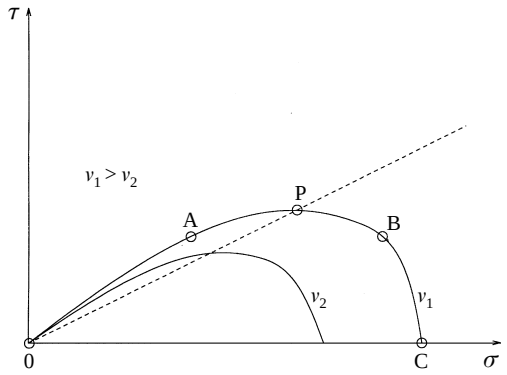

FIGURE 1. Yield locus in the (σ, τ)-plane.

sense from the x-axis. In terms of the Sokolovski variables, the frictional stress tensor can be written as

$$\boldsymbol{\Sigma}_{\mathrm{f}} = \begin{pmatrix} \sigma + \tau\cos(2\gamma) & -\tau\sin(2\gamma) \\ -\tau\sin(2\gamma) & \sigma - \tau\cos(2\gamma) \end{pmatrix}.$$

The constitutive model consists of three components: the yield condition, the condition of coaxiality and the flow rule.

The yield condition for isotropic materials states that if the material deforms, the state of stress is determined by a functional relation of the form

$$\tau = \tau(\sigma, \nu). \tag{2.8}$$

The above equation incorporates the rigid–perfectly plastic approximation which assumes that the material is rigid if τ is less than the threshold $\tau(\sigma, \nu)$, and perfectly plastic in the sense that τ cannot be forced above this threshold. The yield condition may be represented in the (σ, τ)-plane as a set of yield loci, one for each value of ν. For a given density ν_1, the yield locus $\tau(\sigma, \nu_1)$ is convex and is of the general shape shown in figure 1. Points on the yield locus to the left of P (such as A) correspond to dilation, and those to the right of P (such as B) correspond to compaction. Points such as P (where $\partial\tau/\partial\sigma = 0$) correspond to isochoric states, and are known as *critical states*. There is one critical state for every ν, and the locus of critical states for all ν is the critical state line.

The co-axiality condition requires that the principal directions of $\boldsymbol{\Sigma}_{\mathrm{f}}$ and the strain-rate tensor to be aligned, with the major principal stress aligned with the minor principal rate of deformation. If u and v are the Cartesian components of velocity, this condition leads to

$$\cos(2\gamma)\left(\frac{\partial u}{\partial y} + \frac{\partial v}{\partial x}\right) = \sin(2\gamma)\left(\frac{\partial v}{\partial y} - \frac{\partial u}{\partial x}\right). \tag{2.9}$$

The flow rule relates the stress to the rate of deformation, and is expressed as

$$\cos(2\gamma)\left(\frac{\partial u}{\partial x} + \frac{\partial v}{\partial y}\right) = \frac{\partial\tau}{\partial\sigma}\left(\frac{\partial v}{\partial y} - \frac{\partial u}{\partial x}\right). \tag{2.10}$$

The flow rule holds that the material will consolidate or dilate according to whether (σ, τ) lies to the right or left of the critical state line, respectively.

The functional form of τ is taken as (Prakash & Rao 1988)

$$\tau = \sigma_c(\nu)\left(n\alpha - (n-1)\alpha^{n/(n-1)}\right)\sin\phi \tag{2.11}$$

where $\sigma_c(\nu)$ is the mean stress at the critical state for the solids fraction ν, $\alpha = \sigma/\sigma_c(\nu)$ and n is a constant in the range $1 < n < 1/\sin\phi$. The closer n is to unity, the steeper is the compaction branch PBC of the yield locus (figure 1). Jyotsna (1993) fitted a value of 1.03 for n from data on Leighton-Buzzard sand, which we retain in this study. At critical state, the above equation reduces to the well-known Coulomb relationship,

$$\tau_c = \sigma_c \sin\phi,$$

where ϕ is the 'angle of internal friction', a quantity measured in slow plane shearing experiments which characterizes the roughness of the granular medium. Experimental observations on sand (Atkinson & Bransby 1982, p. 240) indicate that σ_c increases rapidly with bulk density. While data for densities close to maximum packing are not available, it is reasonable to assume that σ_c diverges as ν_{max} is approached. A simple algebraic representation of this behaviour is

$$\left.\begin{aligned} \sigma_c(\nu) &= Fr\frac{(\nu-\nu_{min})^{\mathscr{P}}}{(\nu_{max}-\nu)^{\mathscr{N}}} && (\nu > \nu_{min}) \\ &= 0 && (\nu \leqslant \nu_{min}) \end{aligned}\right\}, \tag{2.12}$$

where $Fr = \widetilde{Fr}/\rho_p d_p^2 \tilde{\Gamma}^2$, $\mathscr{N}$, and $\mathscr{P}$ are constants. This model asserts that frictional interactions do not occur at values of $\nu \leqslant \nu_{min}$ for which randomly distributed particles are not in contact. We assume that the critical state model remains valid for more rapid deformations in which collisional interactions also contribute to the total stress. The values of $\widetilde{Fr}$, ϕ, ν_{min}, ν_{max}, $\mathscr{N}$, $\mathscr{P}$, and other parameters are listed in table 2. These were used by Johnson, Nott & Jackson (1990) and Nott & Jackson (1992) for a medium comprising glass beads of 1 mm diameter. We retain the value of n corresponding to sand (see above) as data for glass beads are not available. The results presented in this work are for the parameter set listed in table 2, with the exception of figures 14 and 15 where the sensitivity of the stability results to the angle of internal friction ϕ is explored.

3. Linear stability analysis

We consider the linear stability of unbounded granular shear flow at constant shear rate $\tilde{\Gamma}$ and uniform solids fraction ν^0. Flow is in the x-direction and the velocity gradient is in the y-direction. The solution for the base state is

$$u^0(y) = y, \quad T^0(\nu^0) = f_2(\nu^0)/f_5(\nu^0).$$

The co-axiality condition (2.9) implies that $\gamma^0 = \pi/4$. Since the deformation is isochoric, the material is always at critical state (i.e. $\partial\tau/\partial\sigma = 0$). Therefore the flow rule (2.10) is trivially satisfied.

We look for two-dimensional disturbances of the above base state, such that

$$\begin{aligned} u &= u^0(y) + u'(x,y,t), & v &= v'(x,y,t), \\ \nu &= \nu^0 + \nu'(x,y,t), & T &= T^0 + T'(x,y,t), \\ \boldsymbol{\Sigma}_{\mathrm{k}} &= \boldsymbol{\Sigma}_{\mathrm{k}}^0 + \boldsymbol{\Sigma}_{\mathrm{k}}'(x,y,t), & \boldsymbol{\Sigma}_{\mathrm{f}} &= \boldsymbol{\Sigma}_{\mathrm{f}}^0 + \boldsymbol{\Sigma}_{\mathrm{f}}'(x,y,t), \\ \boldsymbol{q} &= \boldsymbol{q}^0 + \boldsymbol{q}'(x,y,t), & \mathscr{D} &= \mathscr{D}^0 + \mathscr{D}'(x,y,t), \\ \gamma &= \gamma^0 + \gamma'(x,y,t), \end{aligned}$$

where primed quantities stand for infinitesimal perturbations. The perturbation of the frictional stress tensor is derived in the next subsection. We have restricted this study to two-dimensional disturbances as there are insufficient data to formulate with confidence a three-dimensional yield surface.

3.1. *Perturbation of frictional stress tensor,* $\boldsymbol{\Sigma}'_{\mathrm{f}}$

In terms of disturbance variables, the linearized coaxiality condition may be written as

$$\gamma' = \frac{1}{2}\left(\frac{\partial u'}{\partial x} - \frac{\partial v'}{\partial y}\right) \Big/ \left(\frac{\mathrm{d}u^0}{\mathrm{d}y}\right), \tag{3.1}$$

and the linearized flow rule as

$$\frac{\partial \tau}{\partial \sigma} = \left(\frac{\partial v'}{\partial y} + \frac{\partial u'}{\partial x}\right) \Big/ \left(\frac{\mathrm{d}u^0}{\mathrm{d}y}\right). \tag{3.2}$$

The Taylor series expansion of $\partial\tau/\partial\sigma$ about the critical state yields

$$\frac{\partial \tau}{\partial \sigma} = \tau^0_{\sigma\sigma}\sigma' + \tau^0_{\sigma v}v', \tag{3.3}$$

where the subscripts σ and v indicate partial derivatives and the superscript 0 indicates quantities evaluated at base-state conditions. Combining (3.2) and (3.3), the perturbed mean stress becomes

$$\sigma' = \frac{1}{\tau^0_{\sigma\sigma}}\left[\frac{1}{(\mathrm{d}u^0/\mathrm{d}y)}\left(\frac{\partial v'}{\partial y} + \frac{\partial u'}{\partial x}\right) - \tau^0_{\sigma v}v'\right]. \tag{3.4}$$

The perturbation in the shear stress may be obtained from the Taylor series expansion of $\tau(\sigma, v)$ about the base state (σ^0, τ^0, v^0),

$$\tau' = \left(\frac{\partial \tau}{\partial v}\right)^0 v' = \tau^0_v v'. \tag{3.5}$$

In terms of $(\sigma', \tau', \gamma')$, the perturbed frictional stress tensor may be written as

$$\boldsymbol{\Sigma}'_{\mathrm{f}} = \begin{pmatrix} \sigma' - 2\gamma'\tau^0 & -\tau' \\ -\tau' & \sigma' + 2\gamma'\tau^0 \end{pmatrix}. \tag{3.6}$$

Using (3.1), (3.4), and (3.5), $\boldsymbol{\Sigma}'_{\mathrm{f}}$ can be expressed in terms of the primary disturbance variables (v', u', v').

3.2. *Kelvin modes and the linearized evolution equations*

Linearizing the governing equations (2.1)–(2.3) about the steady base state, we obtain a set of linear equations for the infinitesimal disturbance quantities (v', u', v', T'). Since the coefficients of certain terms of the linearized equations depend on the spatial variable y explicitly, we cannot seek solutions in the form of simple plane waves. However, following Moffatt (1967) (and more recently, Savage 1992*b*, Babić 1993 and Schmid & Kytömaa 1994), we seek solutions in the form of Kelvin modes

$$\boldsymbol{X}'(x, y, t) = \boldsymbol{X}(t)\exp\left[\mathrm{i}\boldsymbol{k}(t)\cdot\boldsymbol{x}\right], \tag{3.7}$$

with

$$\boldsymbol{X}' = (v', u', v', T')^T, \quad \boldsymbol{x} = [x, y]^T, \quad \boldsymbol{k}(t) = \left[k_{x0}, k_{y0} - tk_{x0}\right].$$

Here k_{x0} and k_{y0} are the components of the wavenumber vector at $t = 0$. In this model, the disturbances interact with the mean flow in the sense that the wavenumber

vector $\boldsymbol{k}(t)$ is rotated by the mean shear flow. Note that the x-component of $\boldsymbol{k}(t)$ remains constant but the y-component varies linearly with time leading to wavefronts becoming progressively parallel to the x-axis as time increases.

Substituting the above form of Fourier modes into the linearized equations, we get a set of equations for the evolution of the disturbance amplitudes $\hat{v}$, $\hat{u}$, $\hat{v}$, and $\hat{T}$, which may be written as

$$\frac{\mathrm{d}\boldsymbol{X}}{\mathrm{d}t} = \boldsymbol{A}(t)\boldsymbol{X}, \quad \text{with} \quad \boldsymbol{X} = (\hat{v}, \hat{u}, \hat{v}, \hat{T})^T. \tag{3.8}$$

The time-dependent matrix, $\boldsymbol{A}(t)$, can be decomposed as $\boldsymbol{A}(t) = \boldsymbol{A}^k(t) + \boldsymbol{A}^f(t)$, where $\boldsymbol{A}^k(t)$ has entries originating from the kinetic model and $\boldsymbol{A}^f(t)$ arises from the frictional stress in the momentum balance. The elements of $\boldsymbol{A}^k(t)$ and $\boldsymbol{A}^f(t)$ are listed in Appendix A.

For the problem under consideration, $\boldsymbol{A}(t)$ has a quadratic form in time,

$$\boldsymbol{A}(t) = \boldsymbol{A}_0 + \boldsymbol{A}_1 t + \boldsymbol{A}_2 t^2, \tag{3.9}$$

where $\boldsymbol{A}_0$, $\boldsymbol{A}_1$ and $\boldsymbol{A}_2$ are constant matrices. The elements of the matrix $\boldsymbol{A}_0$ are the same as those of $\boldsymbol{A}(t)$ with $k_x = k_{x0}$ and $k_y = k_{y0}$.

4. Asymptotic stability

In this section we present results for the asymptotic stability of (3.8). The inclusion of friction introduces an additional parameter in the governing equations, $Fr = \widetilde{Fr}/\rho_p d_p^2 \tilde{\Gamma}^2$, the non-dimensional friction coefficient. The inverse of Fr is the equivalent of the Reynolds number for quasi-static frictional flows; it is the ratio of inertia and frictional driving forces. However, it is fundamentally different from the Reynolds number for viscous flows in that the frictional stress is rate independent. It is also noteworthy that, when the stress is purely kinetic, there is no Reynolds number occurring in the governing equations, as was pointed out by Wang *et al.* (1996). This is due to the lack of a thermodynamic temperature in granular flows – all the transport properties are proportional to the grain temperature T, which in turn is 'driven' by the imposed flow.

To study the effect of friction on stability, the analysis must be performed for a wide range of Fr. Since we wished to also explore the effect of the solids fraction v^0, the stability analysis was performed for only four representative values of Fr: 3.8×10^{-5}, 9.5×10^{-4}, 1.52×10^{-2} and 0. For the material parameters given in table 2, the first three of the above values of Fr correspond to shear rates of 674, 135 and 34 s^{-1}, respectively, and the last represents the case of a purely kinetic stress. The reason for choosing these values of the shear rate is that they fall within the range for which stress measurements were made by Savage & Sayed (1984). From their data, it appears that the smallest of the above shear rates lies in the quasi-static (rate-independent) regime, and the largest in the 'grain-inertia' regime where the kinetic stress dominates.

Schmid & Kytömaa (1994) determined the evolution of infinitesimal disturbances in the limit of large time by arguing that $\boldsymbol{A}_2 t^2$ determines the asymptotic behaviour of (3.8) since it is the dominant part of $\boldsymbol{A}(t)$. We show below that this assumption leads to an incorrect result and proceed to derive the correct asymptotic behaviour.

Let us for simplicity consider just the linearized y-momentum balance in (3.8),

$$\frac{\mathrm{d}\hat{v}}{\mathrm{d}t} = a_{31}\hat{v} + a_{32}\hat{u} + a_{33}\hat{v} + a_{34}\hat{T}. \tag{4.1}$$

For large time, the variation of the coefficients is such that $a_{33} \sim t^2$ while the other three vary as t (see Appendix A). Schmid & Kytömaa drop the other terms on the right-hand side of (4.1) in favour of the third, the implicit (though unstated) assumption being that the asymptotic dominant balance (Bender & Orszag 1984, p. 83) is between $\mathrm{d}\hat{v}/\mathrm{d}t$ and $a_{33}\hat{v}$. Using the same argument for the x-momentum and energy balances, they derived the asymptotic variation of the disturbance amplitudes as

$$\hat{u} \sim \exp(-C_u t^3), \quad \hat{v} \sim \exp(-C_v t^3), \quad \hat{T} \sim \exp(-C_T t^3) \tag{4.2}$$

where C_u, C_v and C_T are positive real constants, related to the time-independent parts of a_{22}, a_{33} and a_{44}, respectively. If we now substitute (4.2) into the continuity equation in (3.8), we can determine the asymptotic variation of $\hat{v}$ after any suitably large time t_r to be

$$\hat{v} \sim \hat{v}(t_r) + \int_{t_r}^{t} t \exp(-C_v t^3)\,\mathrm{d}t. \tag{4.3}$$

Thus, $\hat{v}$ does not decay with time but is in fact always of the same order as the initial disturbance. When (4.3) is substituted back into (4.1) to check for consistency, we find that the assumed dominant balance is incorrect: $a_{31}\hat{v}$ is asymptotically much greater than $a_{33}\hat{v}$. Therefore, the above result of Schmid & Kytömaa for the asymptotic variation of the disturbances is incorrect.

The proper dominant balance is in fact between the terms on the right-hand side of each of the last three equations in (3.8); for example, the dominant balance for the x-momentum equation in (3.8) is

$$a_{21}\hat{v} + a_{22}\hat{u} + a_{23}\hat{v} + a_{24}\hat{T} \sim 0.$$

These can be rearranged to yield expressions for $\hat{u}$, $\hat{v}$ and $\hat{T}$ in terms of $\hat{v}$, which may then be substituted into the continuity equation to solve for $\hat{v}$. The result then is

$$\left.\begin{aligned} \hat{v}(t) &\sim \exp(-Ct), & \hat{u}(t) &\sim (1/t)\exp(-Ct), \\ \hat{v}(t) &\sim (1/t)\exp(-Ct), & \hat{T}(t) &\sim \exp(-Ct), \end{aligned}\right\} \tag{4.4}$$

where

$$C = v^0 \frac{\left(f_{1v}^0 - f_1^0(f_{4h}^0/f_4^0)\right) T^0 + \sigma_{cv}^0}{\left(f_3^0 + \tfrac{4}{3}f_2^0\right) T^{0\,1/2} + \sigma_c^0 \left(\sin\phi + \dfrac{n-1}{n\sin\phi}\right)} > 0.$$

Here and elsewhere in this paper, f_i^0 refers to the functions f_i (table 1) evaluated at v^0. This solution may be substituted back into (3.8) to verify that the dominant balance we had chosen is indeed consistent.

Since the above asymptotic analysis shows that every Fourier component of an initial disturbance decays as $t \to \infty$, an arbitrary disturbance will decay asymptotically. Therefore, unbounded granular shear flow is stable to infinitesimal disturbances when $k_x \neq 0$ for the kinetic and frictional–kinetic models.

However, the above analysis is not valid for disturbances in the form of layering modes ($k_x = 0$, $k_y \neq 0$) because the adopted dominant balance is no longer correct (the time-dependent coefficients vanish). Wang *et al.* (1996) demonstrated clearly that the flow may become unstable to layering modes for the purely kinetic model. In the following section, the effect of friction on the asymptotic stability of layering modes is assessed.

4.1. *Layering modes ($k_x = 0$, $k_y \neq 0$)*

When k_x is set to zero, the time-dependent part of the linear operator vanishes, leading to a constant matrix $\boldsymbol{A}_0(k_x = 0)$. For this particular case the wave vector $\boldsymbol{k}(t)$ is perpendicular to the x-axis, corresponding to disturbances that do not vary in the streamwise direction. To determine linear stability, we calculate the spectrum of $\boldsymbol{A}_0$, whose real part is the growth rate and the imaginary part is the frequency of the disturbance. The least-stable eigenvalue ω^l is the one with largest real part. If ω_r^l, the real part of the least-stable eigenvalue, is positive, then the infinitesimal disturbance will grow exponentially with time leading to instability. A negative ω_r^l implies that the disturbance decays exponentially. There is a least-stable eigenvalue for every point in the (v_0, k_{y0})-plane. The flow is stable to all disturbances if ω_r^l is not positive for all k_{y0}, and unstable otherwise. If the maximum of ω_r^l over k_{y0} is zero, the flow is said to be neutrally stable. The only material parameter for the kinetic model is e_p, while there is an additional parameter Fr for the frictional–kinetic model. Other frictional parameters are fixed and are listed in table 2; sensitivity of our results to these parameters is discussed in § 6.

At this point, we pause to consider the dependence of the growth (or decay) rates of disturbances on the shear rate. The dimensionless eigenvalues ω are scaled with the shear rate. The results for the kinetic model are valid for all shear rates, since there is no parametric dependence of the dimensionless linearized equations on the shear rate. Hence the dimensional growth (or decay) rate for any shear rate may be obtained by multiplying ω by the shear rate. However, stability results for the frictional–kinetic model depend on the parameter Fr and therefore, for a material with given frictional parameters, on the shear rate. These points must be borne in mind while comparing stability results of the kinetic and frictional–kinetic models. Comparisons are straightforward if the shear rate is thought to be equal in the two cases.

Before discussing the results for layering modes, we look at the trivial case of spatially uniform disturbances. For this case, $k_x = k_y = 0$ and the dispersion relation can readily be obtained. Out of four eigenvalues, three are identically zero and the fourth is negative with a magnitude of $2f_5^0 T^{0\,1/2}/3v^0$. Therefore unbounded granular shear flow is neutrally stable to spatially uniform disturbances. Note that this result is unaffected by the inclusion of friction. The importance of uniform disturbances will be considered in connection with transient behaviour in § 5.2.

4.1.1. *Purely frictional stress*

It is illuminating to consider the case of a purely frictional stress. The equation set now consists of the continuity and two momentum balances with $\boldsymbol{\Sigma}_k = 0$; there is no fluctuational energy balance. For this case, the dispersion relation simplifies to

$$\omega(\omega^2 + c_1^f \omega + c_0^f) = 0,$$

with

$$c_1^f = \frac{1}{v^0}\left(\tau^0 - \frac{1}{\tau_{\sigma\sigma}^0}\right) k_{y0}^2 = \frac{\sigma_c^0}{v^0}\left(\sin\phi + \frac{n-1}{n\sin\phi}\right) k_{y0}^2 > 0,$$

$$c_0^f = -\left(\frac{\tau_{\sigma v}^0}{\tau_{\sigma\sigma}^0}\right) k_{y0}^2 = \sigma_{cv}^0 k_{y0}^2 > 0.$$

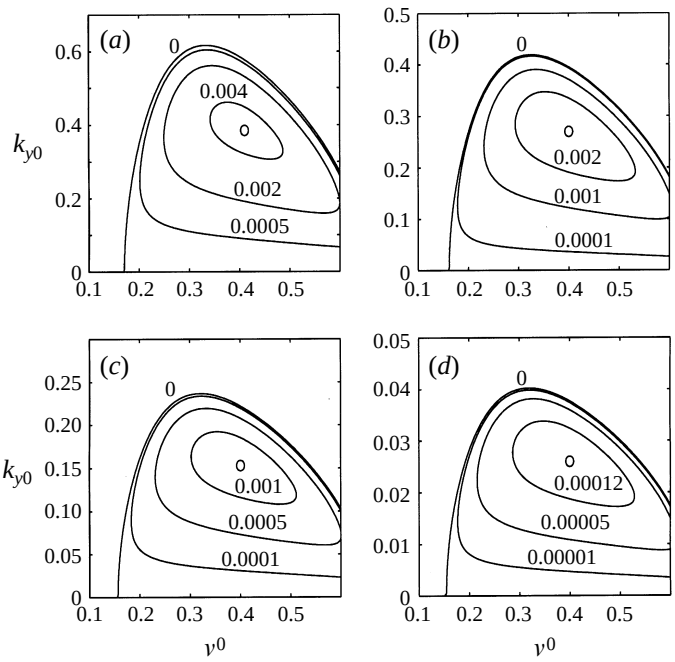

FIGURE 2. Contours of ω_r^l, the real part of the least-stable eigenvalue, for layering modes ($k_{x0} = 0$) in the (v^0, k_{y0})-plane for the purely kinetic model, with the coefficient of restitution e_p set to (*a*) 0.40, (*b*) 0.60, (*c*) 0.80 and (*d*) 0.99.

The roots of the dispersion relation are

$$\omega^{(1,2)} = \tfrac{1}{2}c_1^f\left(-1 \pm \left(1 - 4c_0^f/c_1^{f\,2}\right)^{1/2}\right),$$
$$\omega^{(3)} = 0.$$

Since both c_0^f and c_1^f are positive, the non-zero roots ($\omega^{(1)}$ and $\omega^{(2)}$) are either a pair of complex conjugates with negative real parts or purely real and negative, depending on whether the ratio $4c_0^f/c_1^{f\,2}$ is greater or less than unity, respectively. This makes $\omega^{(3)}$ the least-stable eigenvalue, and hence unbounded shear flow is neutrally stable to disturbances in the form of layering modes for the purely frictional model.

4.1.2. *Kinetic and frictional–kinetic models*

The eigenvalues of the matrix $\boldsymbol{A}_0(k_x = 0)$ were determined using the MATLAB software package on an IBM RS-6000 workstation. Figure 2 shows contours of ω_r^l in the (v^0, k_{y0})-plane for four different values of e_p, for the case of a purely kinetic stress. Inside the $\omega_r^l = 0$ contour (other than at $k_{y0} = 0$), the flow is unstable to infinitesimal disturbances. At a given solids fraction, the range of unstable transverse wavenumber (k_{y0}) as well as the asymptotic growth rate of the least-stable mode decrease as the coefficient of restitution approaches unity, demonstrating the inelastic nature of the instability. The maximum growth rate, indicated by a circle in each plot, seems to occur at a solids fraction of roughly 0.40, and this particular feature does not appear to depend on e_p. Note that the flow is stable in the dilute limit ($v^0 < 0.15$) irrespective of the value of e_p. In this regard, we note that Wang *et al.* (1996) observed that unbounded granular shear flow in the dilute limit is linearly

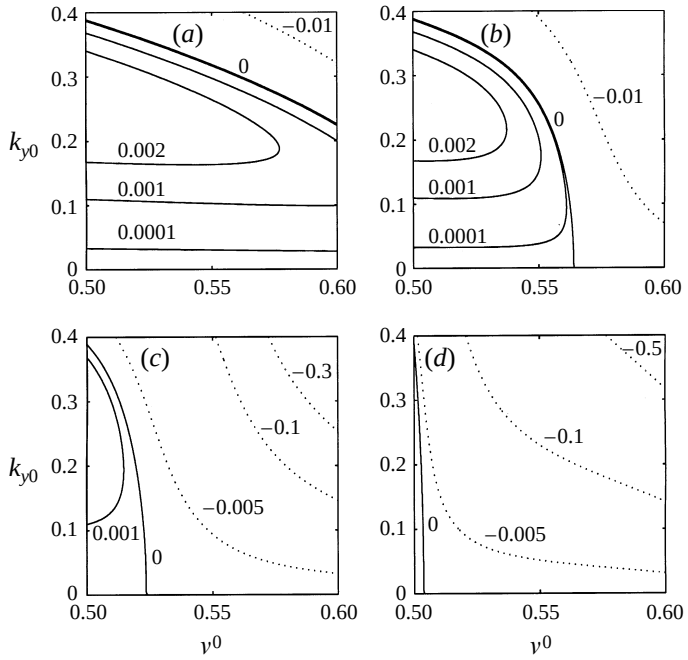

FIGURE 3. Contours of ω_r^l for layering modes for the frictional-kinetic model with $e_p = 0.5$. (*a*) Purely kinetic model; (*b–d*) frictional–kinetic model with the friction coefficient Fr set to (*b*) 3.8×10^{-5}, (*c*) 9.5×10^{-4} and (*d*) 1.52×10^{-2}. The solid and dotted lines represent unstable and stable contours, respectively.

unstable to three-dimensional disturbances with $k_{x0} = 0$; however for $v^0 > 0.25$ the dominant mode was again found to be two-dimensional.

The growth rate contours of the least-stable mode for the frictional–kinetic case are shown in figure 3 for three different values of the friction coefficient, with e_p fixed at 0.50. The effect of friction is felt only when the solids fraction exceeds 0.5, in accordance with the functional form for σ_c in (2.12). The dotted contours represent decay rates in the stable region. At this value of e_p, inclusion of friction tends to stabilize the flow; at $Fr = 1.52 \times 10^{-2}$, the flow becomes stable for all v^0 greater than 0.503.

Friction can have the opposite effect on stability if we increase the value of the coefficient of restitution. To illustrate this, the growth rate contours of the least-stable mode are shown in figure 4 for $e_p = 0.80$. We observe that in the limit of low friction there is very little change in the neutral stability curve, except at densities near maximum packing. As the friction coefficient is increased, we observe an extended region of instability in the (k_{y0}, v^0)-plane. Note that the maximum growth rate is much larger than that in the purely kinetic case.

To further illustrate the effects of the coefficient of restitution and friction on stability, we have shown in figure 5 the variation of ω_r^l with e_p for the purely kinetic and frictional–kinetic models at $v^0 = 0.55$ and $k_{y0} = 0.10$. For the purely kinetic model, the flow is unstable for all values of e_p less than 0.88, and stable beyond that. However, inclusion of friction has the curious effect of stabilizing the flow when e_p is low and enhancing the instability (by increasing the growth rate) when e_p is high. This trend is shown clearly by the dashed line representing $Fr = 9.5 \times 10^{-4}$, for which the flow is stable for e_p less than 0.76 and unstable when e_p is between 0.76 and 0.965.

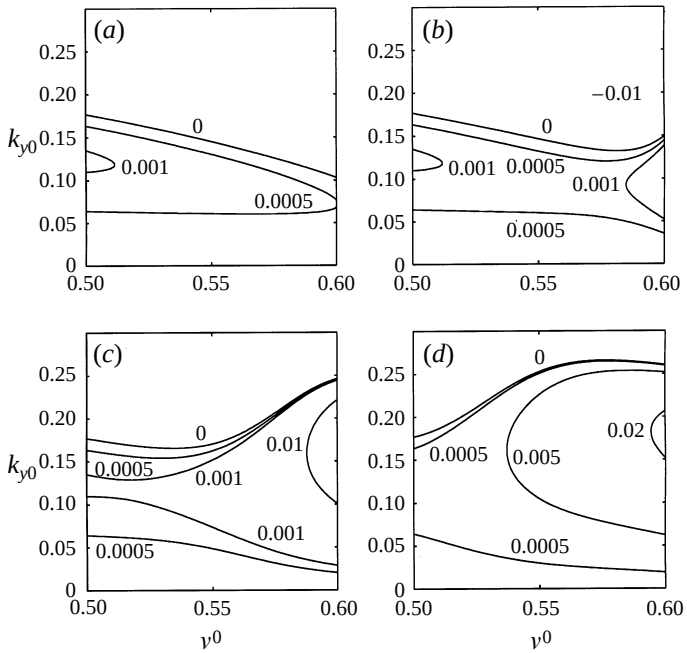

FIGURE 4. Contours of ω_r^l for layering modes for the frictional–kinetic model with $e_p = 0.80$. Other parameters for (a–d) are as in figure 3.

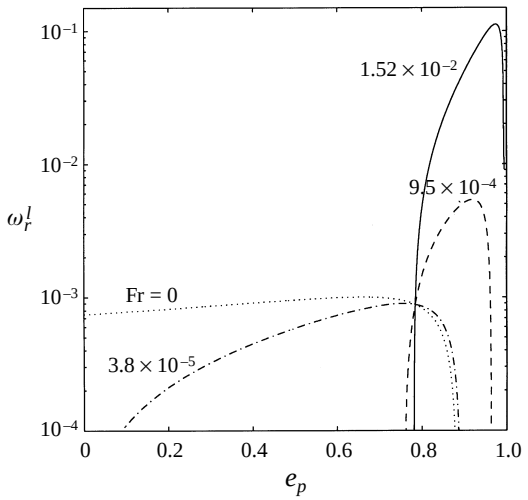

FIGURE 5. Variation of ω_r^l with e_p for the layering mode $k_{x0} = 0$, $k_{y0} = 0.10$, for different values of the friction coefficient Fr at a density of $\nu^0 = 0.55$.

A further increase in Fr to 1.52×10^{-2} makes the flow more unstable (in the unstable range of e_p) in that the growth rate increases by an order of magnitude.

Figure 6(a) traces the location of the four eigenvalues in the complex plane as the coefficient of restitution is varied from 0 to 0.99. Other parameters remain as in the dashed curve of figure 5. There is a pair of complex-conjugate eigenvalues (branches 1 and 2) and two real eigenvalues (branches 3 and 4). The letters A denote the location of eigenvalues at $e_p = 0$ and the letters B give their location

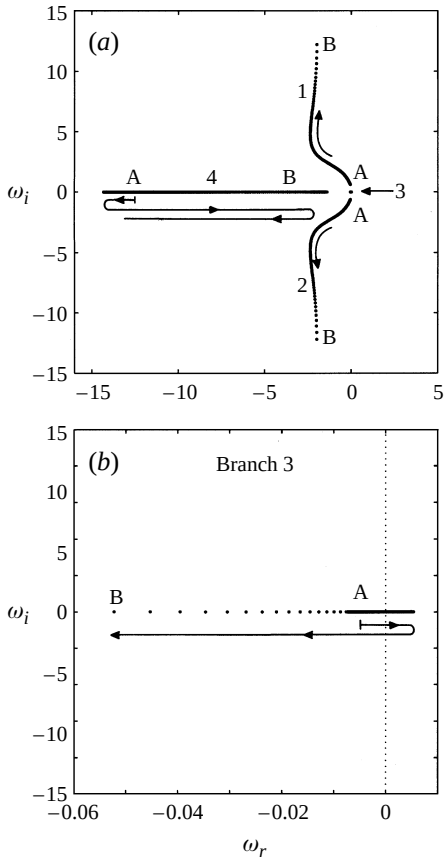

FIGURE 6. The location of the eigenvalues in the complex plane as the coefficient of restitution (e_p) is varied from 0 to 0.99 for the layering mode $k_{x0} = 0$, $k_{y0} = 0.10$. Parameter values are $\nu^0 = 0.55$ and $Fr = 9.5 \times 10^{-4}$. The arrows indicate the direction of increasing e_p. (*b*) An expanded view of branch 3.

at $e_p = 0.99$. The arrows indicate the path of eigenvalues as e_p increases. Branch 3 (see figure 6*b* for an expanded view) is always the least-stable eigenvalue. At this value of the friction coefficient (9.5×10^{-4}), branch 3 starts from the (stable) left half-plane and penetrates into the (unstable) right half, reaches a maximum positive value and then returns to the stable half-plane, moving towards point B. For the purely kinetic model, branch 3 originates in the right half-plane and then follows the same trend. Looking at the frequency of the least-stable mode (imaginary part of the eigenvalue), we find that they are non-oscillatory waves; this is also true for the kinetic model.

The variation of the least-stable eigenvalue with the transverse wavenumber k_{y0} is shown in figure 7. Here the solids fraction is 0.55 and the value of e_p is 0.80. The growth rate corresponding to a friction coefficient of 3.8×10^{-5} is indistinguishable from the dot-dash line, which represents the purely kinetic case. We observe that the asymptotic growth rate increases with k_{y0}, reaching a maximum positive value at some value of k_{y0}, beyond which it decreases monotonically and ultimately becomes negative. The range of transverse wavenumber for which the flow is unstable increases as the friction coefficient increases. We recall that a high friction coefficient corresponds to

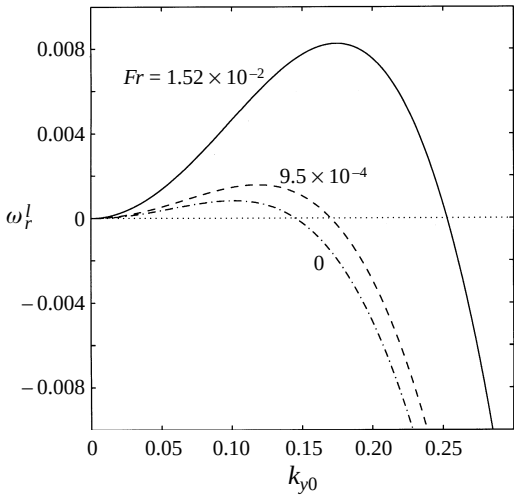

FIGURE 7. Variation of ω_r^l with k_{y0} for layering modes, for different values of Fr. Parameter values are $v^0 = 0.55$ and $e_p = 0.80$.

low shear rate and vice versa. Thus, it appears that friction has negligible effect on the asymptotic growth of infinitesimal disturbances in the rapid flow regime whereas a considerable increase in asymptotic growth rate is possible at low shear rates when $e_p = 0.80$. However, decreasing the value of the coefficient of restitution to 0.5 has the opposite effect on asymptotic growth rate, as can be discerned from figure 3.

Looking at the dependence of the disturbance components on the friction coefficient (details in Alam 1997), we find that fluctuations in the solids fraction are considerably diminished as the friction coefficient is increased. Friction has negligible effect on the streamwise velocity and temperature perturbations, but it affects the transverse velocity mode substantially. We also find that it is the streamwise velocity component which dominates the disturbance structure of the least-stable eigenvectors in the friction-dominated regime.

4.1.3. *Analytical solution for neutral stability*

The dispersion relation for the frictional–kinetic model can be written as

$$\omega^4 + a_3\omega^3 + a_2\omega^2 + a_1\omega + a_0 = 0, \tag{4.5}$$

where the coefficients a_3, a_2, a_1 and a_0 are given in Appendix B. On the neutral stability contour $\omega_r = 0$, the dispersion relation (4.5) becomes

$$\left(\omega_i{}^4 - a_2\omega_i{}^2 + a_0\right) - \mathrm{i}\left(a_3\omega_i{}^2 - a_1\right)\omega_i = 0.$$

From the imaginary part of the above equation, we obtain

$$\omega_i = 0 \quad \text{or} \quad \omega_i{}^2 = a_1/a_3. \tag{4.6}$$

With $\omega_i = 0$ (non-oscillatory modes) the dispersion relation simplifies to

$$a_0 = 0, \tag{4.7}$$

and with $\omega_i{}^2 = a_1/a_3$ (oscillatory modes) the dispersion relation is

$$a_1^2 - a_1a_2a_3 + a_0a_3^2 = 0. \tag{4.8}$$

Equation (4.8) may be simplified to yield a quartic equation in k_{y0}^2, the final form of which is too cumbersome to reproduce here. For all possible parameter combinations, we find that the roots of (4.8) are complex values for k_{y0} which are clearly inadmissible. So we are left with $\omega_i = 0$, i.e. the neutral modes with $\omega_r = 0$ also have $\omega_i = 0$. This implies that the principle of exchange of stabilities (Drazin & Reid 1981, p. 12) holds for layering modes. Therefore to trace the locus of neutral stability, it is sufficient to take $\omega \equiv 0$. After algebraic rearrangement, we get the following equation for the locus of neutral stability:

$$k_{y0}^2 = f_5^0 \left(\frac{N1 + N2 - 2}{N3} \right) \tag{4.9}$$

where

$$N1 = \left(\frac{h_1 + \tau_{cv}^0}{f_2^0 T^{0\,1/2}} \right) \frac{f_1^0 T^0}{h_2} > 0, \quad N2 = \frac{f_{5v}^0}{f_5^0} \frac{f_1^0 T^0}{h_2} > 0, \quad N3 = \left(f_4^0 - \frac{f_1^0 T^0}{h_2} f_{4h}^0 \right) > 0.$$

The coefficients h_1 and h_2 in the above expressions are given in Appendix B. If e_p is fixed, we have instability if (4.9) admits a real solution for k_{y0} at a given value of ν^0. This allows us to trace the neutral stability contour in the (ν^0, k_{y0})-plane. The nature of this instability can be understood if we consider the limit $e_p \to 1$. Since $f_5^0 \to 0$ and $T^0 \to \infty$ as $e_p \to 1$, it follows from (4.9) that $k_{y0} \to 0$, i.e. there is no range of k_{y0} for which the flow is unstable in the elastic limit regardless of the value of the friction coefficient. Therefore, layering instability is driven by the inelasticity of collisions between particles. This result was shown earlier by Babić (1993) for the purely kinetic case; it remains unaltered by the addition of friction.

In figure 2 it is clear that the flow is stable in the dilute limit ($\nu^0 \to 0$). In this limit, $g(\nu) \to 1$ and the non-dimensional functions f_1–f_5 vary as

$$f_1 \sim \nu, \quad f_3 \sim \nu^2, \quad f_5 \sim \nu^2,$$

and f_2, f_4 and f_{4h} tend to constants. It then follows that $N1 \to 0$ and $N2 \to 2$ in this limit. Equation (4.9) then implies that $k_{y0} \to 0$, which means that there is no unstable layering mode in the dilute limit. The critical value of the solids fraction (ν_c^0) below which the flow is stable can be easily obtained by equating the right-hand side of (4.9) to zero. For example, $\nu_c^0 = 0.156$ at $e_p = 0.99$ and $\nu_c^0 = 0.165$ at $e_p = 0.50$. The result that ν_c^0 is not sensitive to e_p follows from the fact that f_1–f_4 are weak functions of e_p.

We recall from § 4.1.2 that inclusion of friction has the curious effect of stabilizing or destabilizing the flow depending on the value of the coefficient of restitution (see figures 3 and 4). This feature can be explained if we consider the behaviour of (4.9) in the regime where the frictional stress dominates. In this regime, $h_1 \approx \tau_v^0$ and $h_2 \approx \sigma_{cv}^0$ (see Appendix B) and it thus follows that

$$N1 \approx 2 \frac{f_1^0}{f_2^0} \sin\phi T^{0\,1/2} \sim \frac{1}{(1 - e_p^2)^{1/2}} \quad \text{and} \quad N2 \approx \frac{f_{5v}^0}{f_5^0} \frac{f_1^0 T^0}{\sigma_{cv}^0} \sim \frac{1}{(1 - e_p^2)\sigma_{cv}^0}.$$

The behaviour of $N1$ is dictated solely by e_p while that of $N2$ is dictated by both Fr and e_p; note also that $N2$ tends to zero when σ_{cv}^0 becomes large. Thus the right-hand side of (4.9) is positive if e_p is large (close to unity), i.e. the flow is unstable. If we decrease the value of e_p, both $N1$ and $N2$ decrease, and we get a threshold for e_p (say e_p^c) at which the right-hand side of (4.9) is identically zero. For $e_p < e_p^c$, $(N1 + N2) < 2$, (4.9) does not admit a real solution for k_{y0} and hence the flow is stable. Thus the strong dependence of $N1$ and $N2$ on e_p is responsible for the observed dual effect

of friction in the frictional–kinetic model. This is in variance with the purely kinetic model for which $N1$ and $N2$ are weak functions of e_p, for the reasons mentioned in the preceding paragraph.

5. Transient behaviour

Thus far we have presented the results for asymptotic stability of unbounded shear flow by considering the spectra of the associated linear operator. For normal operators, the transient behaviour of perturbations is determined solely by the spectra; if all the eigenvalues have negative real parts, then any perturbation will decay monotonically with time. However, if the linear operator is non-normal, transient growth of the disturbance is possible, even if all the individual eigenmodes decay asymptotically. This transient growth is associated with the non-orthogonality of the eigenvectors of the governing linear operator (Reddy, Schmid & Henningson 1993). While transient growth does not imply instability, it does indicate the potential of the flow to amplify disturbances in short time scales. If this transient amplification is substantial, nonlinear effects may take over and ultimately lead to transition to another state. The importance of transient growth for a variety of fluid flows governed by the Orr–Sommerfeld operator has been discussed in recent publications (Butler & Farrell 1992; Reddy & Henningson 1993; Trefethen *et al.* 1993). Here we report the transient behaviour of unbounded shear flow taking into account the frictional stress, following the method of Schmid & Kytömaa. We consider layering and non-layering modes separately in § 5.1 and § 5.2, respectively.

5.1. *Layering modes ($k_x = 0$, $k_y \neq 0$)*

Following Schmid & Kytömaa (1994), we introduce the supremum of the norm of the solution vector over all possible initial disturbances of unit norm as a measure of the size of the disturbances,

$$G(t) \equiv G(t, k_{x0}, k_{y0}, v^0, e_p, Fr) = \sup_{\boldsymbol{X}_0 \neq 0} \frac{\|\boldsymbol{X}\|}{\|\boldsymbol{X}_0\|} = \sup_{\boldsymbol{X}_0 \neq 0} \frac{\|\exp(t\boldsymbol{A}_0)\boldsymbol{X}_0\|}{\|\boldsymbol{X}_0\|} = \|\exp(t\boldsymbol{A}_0)\|.$$

In other words, the growth function $G(t)$ is the largest possible amplification at time t over all initial disturbances of unit norm. We consider disturbance measures in 2-norm, which can be easily calculated using singular value decomposition in MATLAB. Most of the results on transient growth are presented for a fixed value of the coefficient of restitution, $e_p = 0.80$.

Figure 8(a) shows the evolution of the growth function $G(t)$ with time, when $v^0 = 0.55$, $k_{y0} = 0.30$ and $e_p = 0.80$. The dashed line represents results for the purely kinetic model and the solid line for the frictional–kinetic model at a friction coefficient Fr of 1.52×10^{-2}. The flow is asymptotically stable at these conditions. We observe considerable transient growth of disturbances for both cases, though they decay asymptotically. The effect of e_p on transient growth can be inferred by comparing figures 8(a) and 8(b); in the latter, we show the evolution of $G(t)$ at $e_p = 0.50$, other parameters remaining unchanged. We find that a reduction in e_p marginally reduces G_{max}, the temporal maximum of $G(t)$, for the purely kinetic model and marginally increases G_{max} for the frictional–kinetic model. The main difference between the two cases is that $G(t)$ decays at a much faster rate when e_p is reduced to 0.50, for the frictional–kinetic model.

Also of interest is the structure of the disturbances which constitute the maximum transient growth and the effect of friction on it in the frictional regime. To illustrate

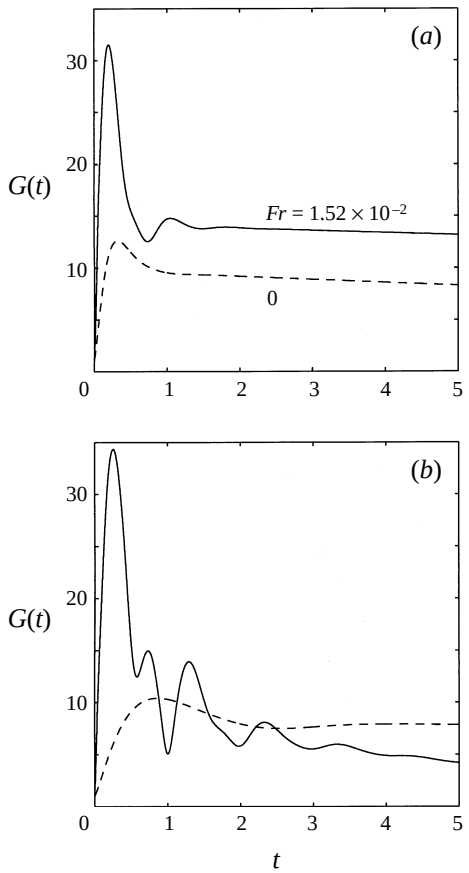

FIGURE 8. Temporal evolution of the growth function $G(t)$ for the layering mode $k_{x0} = 0$, $k_{y0} = 0.30$ for the purely kinetic and frictional–kinetic models. Parameter values are $v^0 = 0.55$ and (*a*) $e_p = 0.80$, (*b*) $e_p = 0.50$.

Disturbance components	Frictional–kinetic model		Kinetic model	
	Optimal mode	Eigenvector	Optimal mode	Eigenvector
$\hat{v}$	1.370×10^{-2}	1.092×10^{-2}	5.099×10^{-2}	3.906×10^{-2}
$\mathrm{i}\hat{u}$	-6.000×10^{-1}	-9.673×10^{-1}	-6.767×10^{-1}	-9.653×10^{-1}
$\mathrm{i}\hat{v}$	7.458×10^{-1}	1.077×10^{-3}	6.529×10^{-1}	7.805×10^{-3}
$\hat{T}$	-2.889×10^{-1}	-2.532×10^{-1}	-3.364×10^{-1}	-2.581×10^{-1}

TABLE 3. Structure of optimal disturbances (figure 8*a*)

this, we have computed the components of the optimal disturbance that will result in the maximum transient growth shown in figure 8(*a*), and the results are tabulated in table 3; for reference, we have also listed the least-stable eigenvector. We observe that for both models the optimal disturbance consists mostly of $\hat{u}$- and $\hat{v}$-waves of comparable magnitudes. It is also noteworthy that the optimal mode differs considerably from the eigenvector of the least-stable mode.

The curves in figure 8 are typical of transient growth of perturbations that are asymptotically stable, in that the growth function increases initially, reaches a maxi-

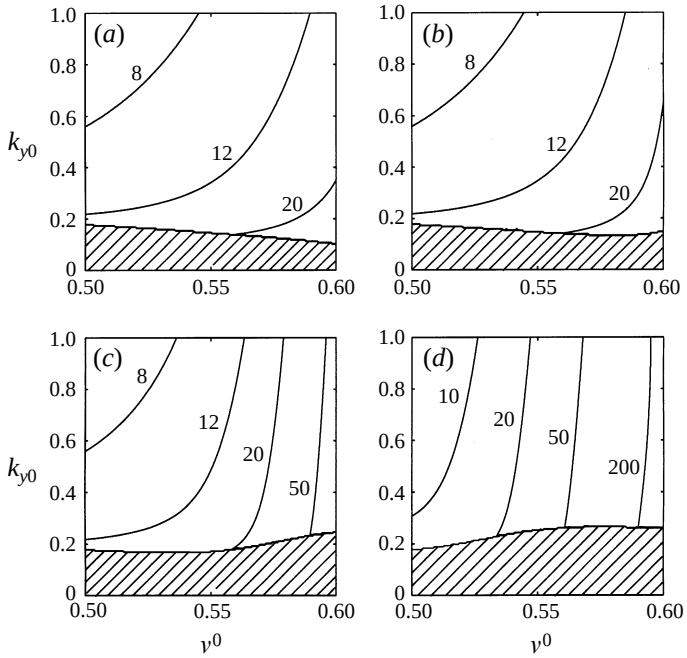

FIGURE 9. Contours of maximum transient growth G_{max} in the (v^0, k_{y0})-plane for layering modes with $e_p = 0.80$. The hatched region represents unstable modes (infinite G_{max}). (*a*) Purely kinetic model; (*b–d*) frictional-kinetic model with (*b*) $Fr = 3.8 \times 10^{-5}$, (*c*) $Fr = 9.5 \times 10^{-4}$ and (*d*) $Fr = 1.52 \times 10^{-2}$.

mum value and then decays asymptotically in the large time limit. Hence, the initial growth rate is an indicator of the importance of transient growth. Following Schmid & Kytömaa, we define the quantity

$$\Omega^i = \frac{1}{\|\boldsymbol{X}\|^2} \frac{\mathrm{d}\|\boldsymbol{X}\|^2}{\mathrm{d}t} \quad \text{at} \quad t = 0 \tag{5.1}$$

as the initial growth rate. Our results show substantial amplification of Ω^i when the friction coefficient Fr is increased, especially when the density is large (see Alam 1997 for details). At a given solids fraction, disturbances of small wavelengths experience larger initial growth rates than those of large wavelengths.

Figure 9 displays contours of the maximum growth over all time, defined as

$$G_{max} \equiv G_{max}(k_{x0}, k_{y0}, v^0, e_p, Fr) = \sup_{t \geqslant 0} G(t),$$

in the (k_{y0}, v^0)-plane. The hatched regions represent points that are asymptotically, unstable, i.e. where infinite amplification is possible due to exponential growth. The contours of G_{max} are unaffected upon inclusion of frictional stress when the friction coefficient is small, except when the solids fraction is high, as shown in figure 9(*b*). At $Fr = 1.52 \times 10^{-2}$, one can achieve substantial amplification of the disturbance norm throughout the (k_{y0}, v^0)-plane. It is interesting to observe that the value of G_{max} decreases as the transverse wavenumber increases. This is in contrast with our earlier observation on initial growth rates; thus, short waves experience maximum initial transient growth rate but long waves are favoured to achieve maximum transient growth.

5.2. *Non-layering modes ($k_x \neq 0$)*

For non-layering modes, the solution of the vector differential equation (3.8) is complicated by the time dependence of the linearized matrix $\boldsymbol{A}(t)$. The solution of (3.8) can be expressed in terms of the fundamental matrix $\boldsymbol{Y}(t)$, which is defined such that $\boldsymbol{X}(t) = \boldsymbol{Y}(t)\boldsymbol{X}(0)$. The fundamental matrix $\boldsymbol{Y}(t)$ satisfies the following matrix differential equation

$$\frac{\mathrm{d}\boldsymbol{Y}}{\mathrm{d}t} = \boldsymbol{A}(t)\boldsymbol{Y}, \quad \boldsymbol{Y}(0) = \boldsymbol{I}, \quad \boldsymbol{A}, \boldsymbol{Y}, \boldsymbol{I} \in \boldsymbol{C}^{4\times 4}, \tag{5.2}$$

where $\boldsymbol{I}$ is the identity matrix.

One can compute the solution of (5.2) by a recurrence technique as discussed in Schmid & Kytömaa (1994), or by the multiplicative integral method as detailed in Gantmacher (1960), or by direct numerical integration. The convergence of the recurrence technique was found to be poor for low values of k_{x0}, and consequently a large number of terms had to be retained for convergence. The multiplicative integral method was better suited for our purpose and we have outlined this technique briefly in Appendix C.

As in the case of layering modes, we define a measure for the size of the disturbance as

$$G(t) \equiv G(t, k_{x0}, k_{y0}, \nu^0, e_p, Fr) = \sup_{\boldsymbol{X}_0 \neq 0} \frac{\|\boldsymbol{X}\|}{\|\boldsymbol{X}_0\|} = \sup_{\boldsymbol{X}_0 \neq 0} \frac{\|\boldsymbol{Y}(t)\boldsymbol{X}_0\|}{\|\boldsymbol{X}_0\|} = \|\boldsymbol{Y}(t)\|.$$

Again, we consider the 2-norm of the fundamental matrix to calculate the growth function $G(t)$.

In figure 10(a) we have displayed $G(t)$ for three values of the friction coefficient Fr at a streamwise wavenumber $k_{x0} = 0.40$; figure 10(b) represents the same at $k_{x0} = 0.08$. The growth curve for the friction coefficient of 3.8×10^{-5} is indistinguishable from that of the purely kinetic case, represented by the dotted line. Note that considerable increase in transient growth is possible for the largest friction coefficient. We observe the appearance of multiple peaks in the growth curve as we decrease the value of the streamwise wavenumber (see figure 10b). It may be noted that for smaller k_{x0}, transient growth persists over a longer period and the maximum in $G(t)$ now occurs at the third peak. This particular feature of multiple peaks in the growth curve is typical of non-layering modes at low k_{x0}. It is interesting to note that transient growth for the frictional–kinetic model decays faster, implying smaller time scales over which fluctuations can occur.

Looking at the dependence of the initial growth rate Ω^i (defined in (5.1)) on the friction coefficient, we find that Ω^i can increase substantially when frictional effects are included. Contours of Ω^i in the (k_{x0}, k_{y0})-plane (see Alam 1997 for details) indicate that disturbances with wave vector inclined at an angle of 45° with the streamwise direction exhibit the smallest initial growth rate. This feature changes neither with Fr nor with solids fraction, as in figure 7 of Schmid & Kytömaa (1994).

To continue further, we define the supremum of G_{max} over all possible k_{y0} at a fixed value of the streamwise wavenumber as the optimal growth:

$$G^{opt} \equiv G^{opt}(t^{opt}, k_{y0}^{opt}) = \sup_{k_{y0}} G_{max}(k_{x0}, k_{y0}, \nu^0, e_p, Fr),$$

where t^{opt} is the time and k_{y0}^{opt} is the transverse wavenumber at which this optimum is achieved. The global optimal transient growth is defined as the supremum of G^{opt} over all k_{x0}.

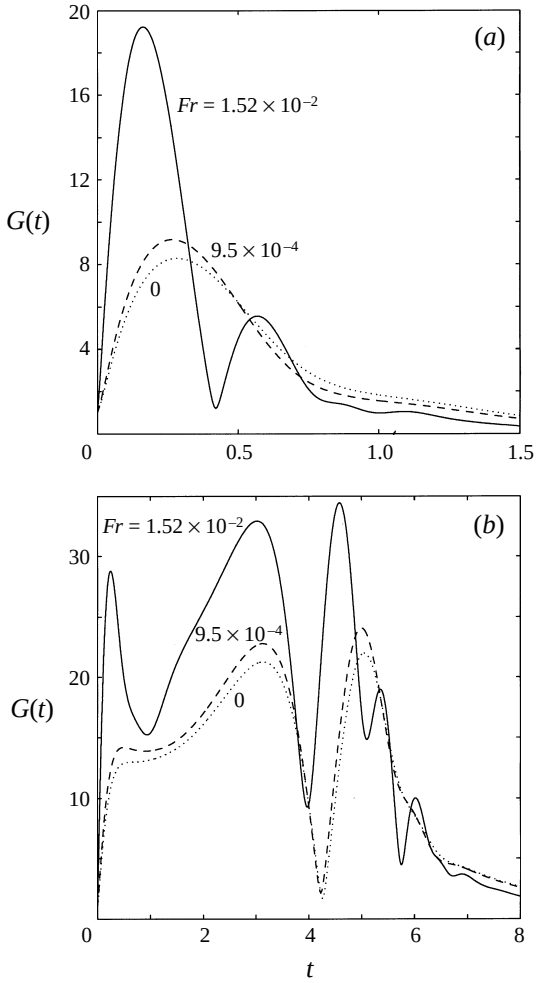

FIGURE 10. Temporal evolution of the growth function $G(t)$ for non-layering modes for three different values of Fr. Parameter values are set to $v^0 = 0.55$, $e_p = 0.80$, $k_{y0} = 0.30$ and (*a*) $k_{x0} = 0.40$, (*b*) $k_{x0} = 0.08$.

In figure 11(*a*), we show contours of the maximum growth, G_{max}, as a function of streamwise and transverse wavenumber for $v^0 = 0.55$, $e_p = 0.80$ and $Fr = 1.52 \times 10^{-2}$; for comparison, the corresponding contour levels for the purely kinetic case are shown in figure 11(*b*). The streamwise wavenumber is varied from 0.01 to 0.2; for larger k_{x0}, G_{max} decreases with k_{x0}. It is clear that there can be significant transient growth throughout the (k_{x0}, k_{y0})-plane even if the flow is linearly stable. We observe that as k_{x0} decreases, the optimal growth increases and the associated optimal transverse wavenumber k_{y0}^{opt} may be positive or negative depending on the value of k_{x0}. Figure 11(*a*) shows that k_{y0}^{opt} is negative when k_{x0} is greater than 0.09, and positive otherwise. Similar trends can be discerned from figure 11(*b*).

To get a better picture of the dependence of the optimal growth on low streamwise wavenumber, we have shown the variation of G_{max} with k_{y0} in figure 12 for two different values of k_{x0} for the purely kinetic case. Other parameters are as in figure 11(*b*). The trends for the frictional–kinetic model are similar. At $k_{x0} = 0.01$, the first peak

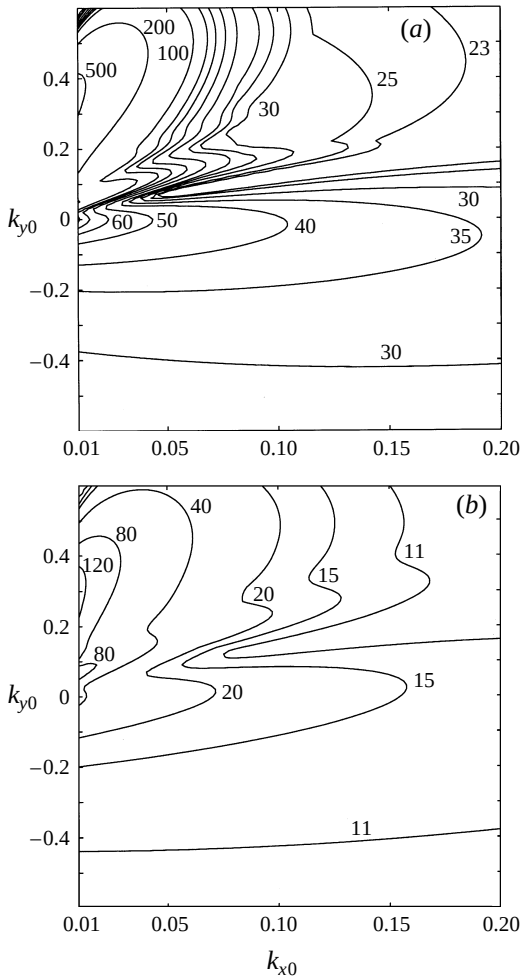

FIGURE 11. Contours of maximum transient growth G_{max} in the (k_{x0}, k_{y0})-plane for non-layering modes. (*a*) Frictional–kinetic model with $Fr = 1.52 \times 10^{-2}$, (*b*) kinetic model. Other parameters are as in figure 10.

near $k_{y0} \approx 0.06$ is dominated by the peak near $k_{y0} \approx 0.3$. As we decrease the value of k_{x0} to 0.001, both the peaks are pushed to lower k_{y0} and, more importantly, the optimal growth now occurs at the first peak near $k_{y0} = 0.02$. The shift of k_{y0}^{opt} towards a lower value may be discerned from table 4 where we have listed G^{opt}, t^{opt} and k_{y0}^{opt} for three different streamwise wavenumbers. The values of v^0 and e_p are the same as in figure 11. It is clear that the optimal growth is likely to occur at arbitrarily small values of k_{x0} for both the models. Note also that the location of G^{opt} appears to be attracted towards $k_{x0} = k_{y0} = 0$. This particular feature can be explained if we consider the evolution of disturbances which do not depend on space.

For spatially uniform disturbances ($k_x = k_y = 0$), the following linear evolution equations govern the behaviour of (not necessarily infinitesimal) disturbances:

$$\mathrm{d}v'/\mathrm{d}t = 0, \tag{5.3}$$

$$\mathrm{d}u'/\mathrm{d}t + u_y^0 v' = 0, \tag{5.4}$$

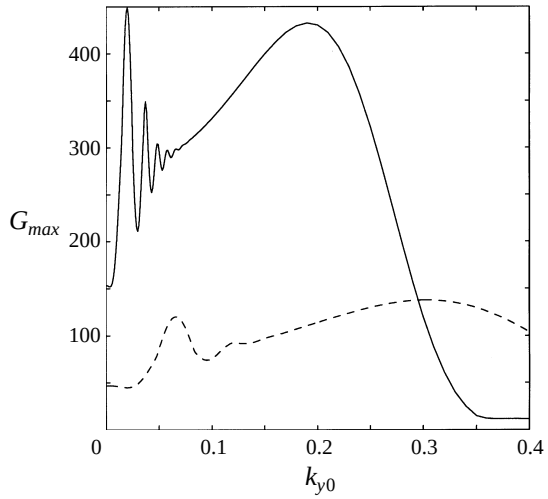

FIGURE 12. Variation of maximum transient growth G_{max} with the transverse wavenumber k_{y0} for the kinetic model. The solid and dashed lines represent streamwise wavenumbers of 0.001 and 0.01 respectively. The solids fraction ν^0 is 0.55 and the coefficient of restitution e_p is 0.80.

	Frictional–kinetic model ($Fr = 1.52 \times 10^{-2}$)			Kinetic model		
k_{x0}	G^{opt}	t^{opt}	k_{y0}^{opt}	G^{opt}	t^{opt}	k_{y0}^{opt}
0.05	1.511×10^2	1.105×10^1	4.87×10^{-1}	5.110×10^1	1.062×10^1	4.35×10^{-1}
0.01	5.787×10^2	4.020×10^1	3.60×10^{-1}	1.376×10^2	3.642×10^1	3.05×10^{-1}
0.001	4.142×10^3	2.894×10^2	2.73×10^{-1}	4.491×10^2	2.704×10^1	2.00×10^{-2}

TABLE 4. Variation of G^{opt}, t^{opt} and k_{y0}^{opt} with streamwise wavenumber

$$\mathrm{d}v'/\mathrm{d}t = 0, \tag{5.5}$$

$$\mathrm{d}T'/\mathrm{d}t + \beta_2 T' - \beta_1 v' = 0, \tag{5.6}$$

where

$$\beta_1 = \frac{2}{3\nu^0}\left(f_{2v}^0 - f_{5v}^0 T^0\right) T^{0\,1/2} \quad \text{and} \quad \beta_2 = \frac{2}{3\nu^0} f_5^0 T^{0\,1/2} > 0.$$

The above set of equations can be immediately integrated to give

$$v'(t) = v'(0), \tag{5.7}$$

$$u'(t) = u'(0) - v'(0)\, u_y^0\, t, \tag{5.8}$$

$$v'(t) = v'(0), \tag{5.9}$$

$$T'(t) = T'(0)\mathrm{e}^{-\beta_2 t} + v'(0)\left(1 - \mathrm{e}^{-\beta_2 t}\right)\beta_1/\beta_2. \tag{5.10}$$

For non-zero $v'(0)$ and u_y^0, the streamwise velocity disturbance increases linearly with time. This is an *algebraic instability*, a term coined by Landhal (1980) in connection with the stability of inviscid parallel shear flows. Note that this result holds for any parallel shear flow, irrespective of whether it is a granular or Newtonian fluid. The

	Frictional–kinetic model ($Fr = 1.52 \times 10^{-2}$)		Kinetic model	
Disturbance components	Optimal mode at $t = 0$	Optimal mode at $t = t^{opt}$	Optimal mode at $t = 0$	Optimal mode at $t = t^{opt}$
$\hat{v}$	9.980×10^{-1}	-7.058×10^{-3}	9.975×10^{-1}	-1.025×10^{-2}
$\mathrm{i}\hat{u}$	-5.527×10^{-2}	8.722×10^{-1}	-6.285×10^{-2}	9.304×10^{-1}
$\mathrm{i}\hat{v}$	-2.489×10^{-2}	-4.842×10^{-1}	-2.728×10^{-2}	-3.560×10^{-1}
$\hat{T}$	-1.408×10^{-2}	-6.834×10^{-2}	-1.341×10^{-2}	-8.631×10^{-2}

TABLE 5. Optimal initial disturbance and its subsequent evolution

behaviour of the disturbance norm at large time is hence

$$G(t) \sim v'(0)\, u_y^0\, t \to \infty \quad \text{as} \quad t \to \infty, \tag{5.11}$$

i.e. the 2-norm of a spatially uniform disturbance with $v'(0) \neq 0$ will grow linearly with time. Therefore the global optimal growth (supremum of G_{max} over k_{x0} and k_{y0}) will occur at $(k_{x0} = 0, k_{y0} = 0)$.

In view of above findings, a discussion of the results of Schmid & Kytömaa (1994) regarding the largest transient growth is in order. They showed that the largest linear growth (global optimum) occurs for very small values of k_{x0} and at a transverse wavenumber of $k_{y0} \approx 0.3$. However a closer look at their figure 10 reveals that they terminated their computations at about $k_{x0} \approx 0.05$. A further decrease in k_{x0} would have revealed the correct picture regarding the location of the global optimal transient growth, which should be attracted towards $k_{x0} = k_{y0} = 0$. For instance our computation for the parameter set of their figure 10(*a*) gives an optimal growth of roughly 70 at $k_{x0} = 0.01$ with the associated transverse wavenumber $k_{y0}^{opt} \approx 0.125$.

We turn now to determine the evolution of the structure of disturbances in time. For this, we focus on the disturbances that achieve the largest amplification in time for given parameter combinations. The initial condition that results in the optimal growth at $k_{x0} = 0.01$ and $v^0 = 0.55$ are shown in table 5 for both the models along with the disturbance components at optimal growth. It is clear that the structure of the initial 'optimal' mode is dominated by the disturbance in solids fraction for both the models; at $t = t^{opt}$, however, it is the streamwise velocity which dominates the structure of the disturbance. To determine which flow variable is most amplified, one has to multiply the ratio of the respective disturbance components at $t = t^{opt}$ and $t = 0$ by G^{opt}. For example, at $t = t^{opt}$ the disturbance in solids fraction will be amplified by a factor of approximately 4.1 and 1.4 for the frictional–kinetic and kinetic models, respectively.

Figures 13(*a*) and 13(*b*) show the initial and optimal solids fraction distribution corresponding to the optimal mode for the frictional–kinetic model given in table 5. On the grey scale, black represents maximum density and white minimum; the contours are drawn at equal intervals of solids fraction. The initial wavenumber combination $(0.01, 0.36)$ corresponds to a wavelength of 17.4 particle diameters, with the wavefronts inclined at an angle of 178.4° from the x-axis. To show this band structure clearly we have used a box of aspect ratio 10 and hence this figure does not show the true inclination angle of the bands, which are actually almost parallel to the x-axis. It is clear that the wavefronts are initially aligned 'against' the shear. Subsequent evolution of the solids fraction field at $t = t_{opt}$ is shown in figure 13(*b*).

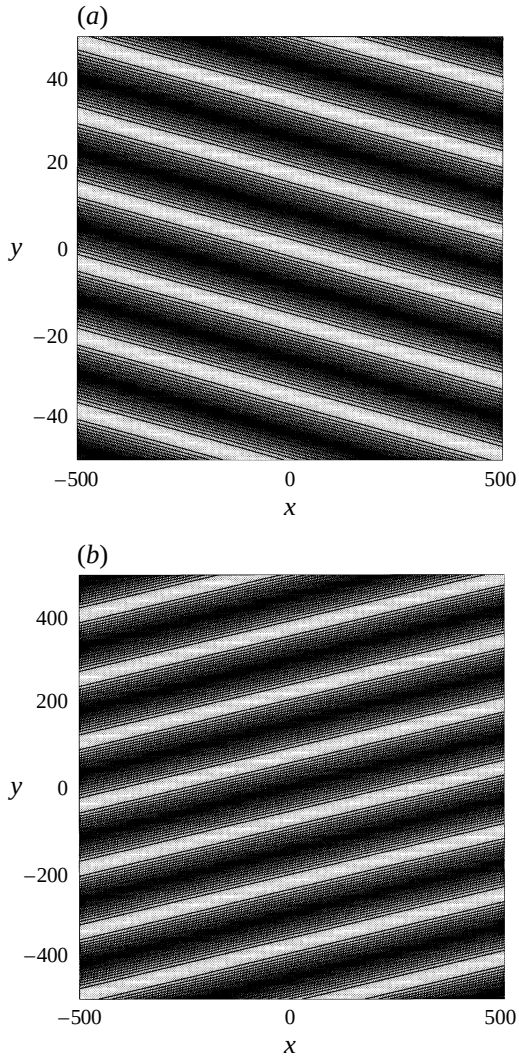

FIGURE 13. The solids fraction disturbance field for the optimal disturbance $k_{x0} = 0.01$, $k_{y0} = 0.360$ at (*a*) $t = 0$ and (*b*) $t = t^{opt}$. Parameter values are $v^0 = 0.55$, $e_p = 0.80$ and $Fr = 1.52 \times 10^{-2}$. On the grey scale, black represents maximum density and white minimum.

Owing to the continual rotation of the wave vector, the transverse wavenumber becomes negative at this time. Consequently the alternating bands of clusters are now turned 'into' the shear and are inclined at an angle 13.5° to the x-axis, and the wavelength now is 145 particle diameters. At later times, these clusters experience stretching in the streamwise direction and this eventually leads to homogeneous layers almost parallel to the flow direction. The optimal disturbance field of solids fraction for the kinetic model at the same parameter values was found to be similar.

6. Discussion

The linear stability of unbounded granular shear flow was considered, using a model for the stress that integrates effects of stress generation due to grain friction

with the kinetic stress that arises from streaming and collisions of grains. Solutions of the linearized equations were sought in the form of Kelvin modes, whose wave vector continually rotates with time. The magnitude of the frictional stress in comparison with other forces is determined by the parameter Fr, which varies as the inverse of the square of the shear rate. Thus, the frictional stress will dominate at low shear rate and the kinetic stress at high shear rate. If a purely frictional stress is assumed, the flow is neutrally stable. When the kinetic stress is also accounted for, the flow may become unstable to disturbances that have no variation in the streamwise direction, i.e. layering modes.

Given that unbounded shear flow of a granular material can become unstable to disturbances of the layering kind, it is clearly of interest to identify the factors in the model that cause instability and those that resist it. An important factor can be readily identified by considering the dependence of k_{y0}^2 on e_p in (4.9). Apart from its weak dependence on e_p through the functions f_1–f_4, k_{y0}^2 varies as $(1-e_p^2)$ through f_5. This suggests that the fluctuational energy balance has an important role to play in causing instability, as f_5 determines the inelastic dissipation rate. This is more clearly illustrated if the linearized energy balance were to be deleted altogether from the system of equations in (3.8) and the temperature perturbation T' set to zero. The dispersion relation for layering modes in this case is a cubic in ω; two roots form a complex-conjugate pair with a negative real part and the third is real and negative. Thus the flow is never unstable if the energy balance is not considered.

Another important factor in whose absence there is no instability is the compressibility of the material. This can be easily verified by keeping the density constant in the governing equations and instead treating the pressure p as another variable. On eliminating the streamwise velocity from the linearized equations by using the continuity equation, we get a system of three equations in place of (3.8) that determines the evolution of the disturbance amplitudes $\hat{v}$, $\hat{p}$ and $\hat{T}$. In the same manner as in §4, it can be shown that the leading-order asymptotic behaviour of these is

$$\left.\begin{array}{ll} \hat{u}(t) \sim t\exp(-Ct^3), & \hat{v}(t) \sim \exp(-Ct^3), \\ \hat{T}(t) \sim \exp(-Ct^3), & \hat{p}(t) \sim (1/t)\exp(-Ct^3), \end{array}\right\} \tag{6.1}$$

where

$$C = \frac{1}{3v^0} f_2^0 T^{0\,1/2} k_{x0}^2.$$

Therefore incompressible shear flow is stable to non-layering modes. (Indeed, disturbances decay even faster than in the compressible case.) For layering disturbances the above asymptotic behaviour no longer holds and (as in the compressible case) stability is determined by the eigenvalues of the constant matrix $\boldsymbol{A}_0$. In this case the linearized momentum balances can be combined into a single balance for the vorticity. Along with the linerized balance of fluctuational energy, this yields a quadratic dispersion relation (see Appendix B). It can be easily checked that both roots have negative real parts and hence the flow is also stable to layering modes in the incompressible limit. It is then clear that compressibility is an essential factor for instability.

It thus appears that instability is caused by an imbalance between the production of fluctuational energy by shear work and its dissipation by inelastic collisions between grains. However, the imbalance never grows to become unstable unless the compressibility of the granular material is accounted for. In this regard, it is interesting to note that the function f_4, which determines the pseudo-thermal conductivity, appears only in denominator of (4.9) and not in the numerator. This

implies that the pseudo-thermal conductivity plays no role in determining the onset of instability. However, our computations indicate that it contributes to reducing the asymptotic growth rate of disturbances, and is therefore a stabilizing influence.

While it is clear that instability can arise only from an imbalance in the energy equation, it can be amplified or suppressed by the inclusion of the frictional stress, which does not appear in the energy balance at all. This is due to the coupling between the momentum and energy balances through the grain temperature T. As is clear from our discussion in §4, increasing Fr stabilizes the flow at low e_p and destabilizes it at larger e_p. However, this result is specific to the chosen value of the angle of internal friction ϕ (cf. table 2). We demonstrate below that this is not necessarily the case for all values of ϕ. A notable point is that unbounded shear flow in the limit of perfectly elastic collisions ($e_p = 1$) is stable regardless of the value of the friction coefficient.

The angle of internal friction is an important frictional property and its influence on stability is clearly of interest. This can be assessed easily if we first recast (4.9) into the following form:

$$\beta k_{y0}^2 = (f_{2v}^0 T^{0\,1/2} + 2\tau_v^0) f_1^0 T^0 + \left(f_{5v}^0/f_5^0\right) f_1^0 f_2^0 T^{0\,3/2} - 2(f_{1v}^0 T^0 + \sigma_{cv}^0) f_2^0 T^{0\,1/2}, \qquad (6.2)$$

where

$$\beta = \left(f_4^0 - \frac{f_1^0 T^0}{(f_{1v}^0 T^0 + \sigma_{cv}^0)} f_{4h}^0\right)(f_{1v}^0 T^0 + \sigma_{cv}^0)\frac{f_2^0 T^{0\,1/2}}{f_5^0}.$$

Note that all three terms on the right-hand side of (6.2) are monotonic increasing functions of v^0. If the angle of internal friction ϕ is increased (keeping all other parameters constant) the frictional shear stress τ increases and so does the first term on the right-hand side of (6.2), while the other two remain unchanged. This implies that in a scenario such as in figure 3 where the flow is stable for solids fractions above a critical value, increasing the roughness of the material results in broadening the range of v^0 for which unbounded shear is unstable. Our computations show in general a rise in the growth rate of disturbances with increasing ϕ. This is clearly shown in figure 14, where contours of the dominant eigenvalue, defined as

$$\omega^d = \sup_{k_{y0}} \omega_r^l,$$

are given in the (v^0, ϕ)-plane with $e_p = 0.50$ and other material properties (with the exception of ϕ) given in table 2. These observations indicate that the material roughness, characterized by the angle of internal friction ϕ, is a destabilizing influence on unbounded shear flow.

Figure 14 also illustrates another interesting dichotomy: increasing the value of Fr does not always stabilize the flow when $e_p = 0.5$. When ϕ is large, increasing Fr actually has a destabilizing effect. Below a critical value ϕ_c, which appears to be a very weak function of v^0 and is roughly 43°, increasing Fr has a stabilizing effect. This qualitative picture also holds when e_p is 0.8, as shown in figure 15, with the important difference that ϕ_c is now much lower at roughly 27.5°. For our computations in §4, ϕ was set to 28.5°, which is just above the critical value for $e_p = 0.8$ and well below that for $e_p = 0.5$. Thus the effect of Fr on stability depends not just on e_p but also on ϕ. A good estimate of the critical value ϕ_c can be made by considering (6.2) in the dense limit. If e_p is not too close to unity, the kinetic stress is small in comparison

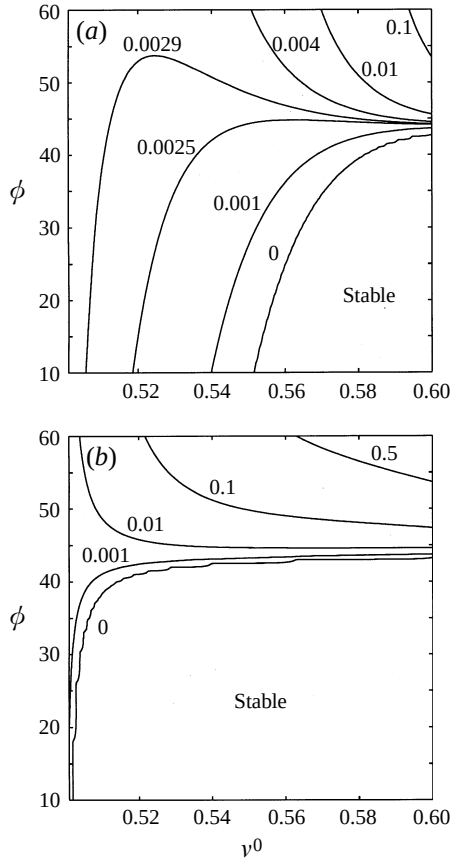

FIGURE 14. Contours of ω^d, the dominant eigenvalue, in the (v^0, ϕ)-plane for the frictional–kinetic model with the friction coefficient Fr set to (*a*) 3.8×10^{-5} and (*b*) 1.52×10^{-2}. Note that ω^d is the supremum over all k_{y0} of least-stable modes. The coefficient of restitution is set to 0.50.

with the frictional stress and hence at neutral stability,

$$\sin\phi_c = \lim_{v \to v_{max}} \frac{(f_2^0 f_5^0)^{1/2}}{f_1^0} = \left(\frac{2(2+\alpha)}{5\pi} \left(\frac{\pi}{3} \frac{(3\eta - 2)}{(2-\eta)} + 4 \right) (1-\eta) \right)^{1/2}. \qquad (6.3)$$

This gives $\phi_c = 27.54^\circ$ at $e_p = 0.80$ and $\phi_c = 43.6^\circ$ at $e_p = 0.50$. Another feature we observe in figures 14 and 15 is that when the material roughness is small and the density large, the flow is always stable.

The result that unbounded shear flow is asymptotically stable when disturbances are in the form of non-layering modes does not imply that these disturbances decay monotonically in time. There can be substantial transient growth of disturbances because the associated linear operator is non-normal. Transient growth of disturbances may be important as it is a possible route by which nonlinearities in the governing equations become dominant and lead to finite-amplitude structures. This was shown to be the case by Butler & Farrell (1994) for viscous shear flows, where they started with an initial perturbation that was known to yield significant transient amplification in the linear regime and showed its rapid evolution into quasi-steady finite-amplitude structures. We have shown that friction has the effect of enhancing the initial growth rate Ω^i as well as the maximum transient growth G_{max}, especially at high solids

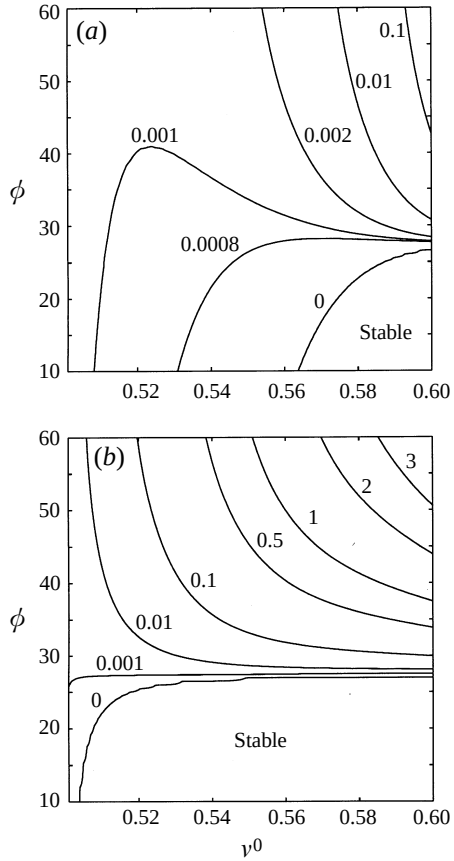

FIGURE 15. Same as figure 14 but with $e_p = 0.80$.

fraction. Interestingly, friction also increases the rate of asymptotic decay for stable flows; thus, disturbances grow faster initially and to levels higher than that in the purely kinetic case, but they also decay faster subsequently. The maximum transient growth for non-layering modes appears to occur for disturbances with wavenumbers $(k_x, k_y) \to 0$.

At this juncture, it is important to note that the results on stability presented in this work are not just valid for the specific forms of the constitutive models for the kinetic and frictional stresses that we have employed and that there is some generality in them. While there is uncertainty in some aspects of the critical-state model for the frictional stress, such as the assumption of coaxiality and the use of an associated flow rule, it is perhaps the most widely used model for quasi-static granular flow. If these assumptions were to be relaxed, for example by eschewing the principle of coaxiality, we believe that the stability results would not qualitatively differ. This is because the two main aspects of the frictional stress that have determined stability are (*a*) that it is rate independent and (*b*) that it does not enter the balance for fluctuational energy. These aspects would remain even if the above changes in the model were made. The components of the model that are susceptible to modification are the functional forms for $\sigma_c(\nu)$ and $\tau(\sigma, \nu)$ in (2.12) and (2.11), respectively. Modifications of these will again leave the qualitative picture of stability unaltered because the main features of the two functions that have influenced stability in this work, that

σ_c diverges as $v \to v_{max}$ and that the yield locus is convex, must remain unchanged (Jackson 1986). Similarly, changes in the transport coefficients in the kinetic model will not qualitatively alter the results as long as their low-v limit remains unaltered and they diverge as $v \to v_{max}$. These arguments are substantiated by the fact that we could detect no appreciable changes in the stability results when we used the form for $\sigma_c(v)$ given by Johnson & Jackson (1987),

$$\sigma_c(v) = \frac{Fr}{(v_{max} - v)^{40}} \qquad (v_{max} > v > 0), \tag{6.4}$$

instead of (2.12), or the Carnahan–Starling radial distribution function at contact used by Savage (1992*b*),

$$g(v) = \frac{2 - v}{2(1 - v)^3}, \tag{6.5}$$

instead of (2.7). Details of these computations may be found in Alam (1997).

Our results indicate that the purely frictional quasi-static shear flow is neutrally stable, although large transient amplification of disturbances can be expected. We are unaware of microstructures reported in simulation studies of unbounded flow that have accounted for friction in particle interactions, and hence no comparison is possible. In practical instances of quasi-static flow, it is well known that shearing is often restricted to thin layers while the rest of the material remains unyielded. In these instances, however, one starts with the material at rest initially and not in a state of uniform shear. Further, the density of the material may not be uniform owing to gravitational compaction. The findings of this study are therefore not directly applicable to these cases. In this regard, it would be a worthwhile effort to extend the study of Wang *et al.* to bounded shear flow including the effects of friction and gravity, complemented by dynamic simulations of the same. The differences in stability between the purely frictional model and the frictional–kinetic model in the limit $Fr \to \infty$ (the former is neutrally stable while the latter may be unstable) are due to the simple manner in which the two modes of stress generation were combined. While the former does not require a balance for fluctuational energy, the latter does. These results point to the necessity for a better model that combines the two mechanisms of momentum transfer.

An important issue is the relationship between stability studies such as this and computer simulations, such as that of Hopkins & Louge (1991). Babić (1993) recognized that the use of periodic boundaries in the latter constrains the wavenumbers to only a discrete set. He correctly pointed out that the wavenumbers in the streamwise and transverse directions belong to the set $2\pi n_1/L_x$ and $2\pi n_2/L_y$, respectively, if L_x and L_y are the dimensions of the periodic domain, and n_1 and n_2 are any integers. Babić also contended that n_1 and n_2 could not be zero, and the minimum wavenumbers were therefore $2\pi/L_y$ and $2\pi/L_x$. This is incorrect, as the only constraint from periodic boundaries is that the quantity $k_x(L_x + L_y t) + k_y L_y$ be an integral multiple of 2π, including zero. This is indeed satisfied by $k_x = 0$ and k_y being an integral multiple of $2\pi/L_y$. Physically, this means that periodic boundaries allow structures that have no variation in the streamwise direction, which is clearly obvious. Thus, it appears that instabilities in the form of layering modes can indeed be picked up by simulations with periodic boundaries.

The clusters observed by Hopkins & Louge (1991) are, however, not layered in the streamwise direction but appear to be oriented along the principal deformation axis and convected by the mean flow. This may be a result of transient amplification of

disturbances, leading to nonlinear effects gaining importance and ultimately resulting in the observed structures. It may also be the case, as suggested by Wang *et al.* (1996), that the microstructure observed by Hopkins & Louge is fluctuations triggered by random noise inherent in simulations and not true instabilities. This can perhaps be verified by conducting the simulations for long periods of time and inferring the structure at various intervals, to see if it remains the same or is altered between intervals.

We wish to acknowledge and thank Professor Vijay H. Arakeri for our many discussions and his useful suggestions. We also wish to acknowledge the Supercomputer Education and Research Center at the Indian Institute of Science for providing computational facilities for this study. M.A. gratefully acknowledges partial support from the Jawharlal Nehru Center for Advanced Scientific Research, Bangalore through a Project Assistantship.

Appendix A. Elements of $\boldsymbol{A}^f(t)$ and $\boldsymbol{A}^k(t)$

The non-zero elements of $\boldsymbol{A}^f(t)$ are

$$a^f(2,1) = \frac{\mathrm{i}}{v^0}\left(\frac{\tau^0_{\sigma v}}{\tau^0_{\sigma\sigma}}k_x + \tau^0_v k_y\right), \quad a^f(2,2) = -\frac{1}{v^0}\left(\tau^0 - \frac{1}{\tau^0_{\sigma\sigma}}\right)k_x^2,$$
$$a^f(2,3) = \frac{1}{v^0}\left(\tau^0 + \frac{1}{\tau^0_{\sigma\sigma}}\right)k_x k_y, \quad a^f(3,1) = \frac{\mathrm{i}}{v^0}\left(\tau^0_v k_x + \frac{\tau^0_{\sigma v}}{\tau^0_{\sigma\sigma}}k_y\right),$$
$$a^f(3,2) = \frac{1}{v^0}\left(\tau^0 + \frac{1}{\tau^0_{\sigma\sigma}}\right)k_x k_y, \quad a^f(3,3) = -\frac{1}{v^0}\left(\tau^0 - \frac{1}{\tau^0_{\sigma\sigma}}\right)k_y^2,$$

and the non-zero elements of $\boldsymbol{A}^k(t)$ are

$$a^k(1,2) = -\mathrm{i}v^0 k_x, \quad a^k(1,3) = -\mathrm{i}v^0 k_y,$$
$$a^k(2,1) = -(\mathrm{i}/v^0)\left(f^0_{1v}T^0 k_x - f^0_{2v}T^{0^{1/2}}k_y\right),$$
$$a^k(2,2) = -(1/v^0)\left(\left(f^0_3 + \tfrac{4}{3}f^0_2\right)k_x^2 + f^0_2 k_y^2\right)T^{0^{1/2}},$$
$$a^k(2,3) = -(1/v^0)\left(f^0_3 + \tfrac{1}{3}f^0_2\right)T^{0^{1/2}}k_x k_y - 1.0,$$
$$a^k(2,4) = -(\mathrm{i}/v^0)\left(f^0_1 k_x - \frac{f^0_2}{2T^{0^{1/2}}}k_y\right),$$
$$a^k(3,1) = (\mathrm{i}/v^0)\left(f^0_{2v}T^{0^{1/2}}k_x - f^0_{1v}T^0 k_y\right),$$
$$a^k(3,2) = -(1/v^0)\left(f^0_3 + \tfrac{1}{3}f^0_2\right)T^{0^{1/2}}k_x k_y,$$
$$a^k(3,3) = -(1/v^0)\left(f^0_2 T^{0^{1/2}}k_x^2 + \left(f^0_3 + \tfrac{4}{3}f^0_2\right)T^{0^{1/2}}k_y^2\right),$$
$$a^k(3,4) = (\mathrm{i}/v^0)\left(\frac{f^0_2}{2T^{0^{1/2}}}k_x - f^0_1 k_y\right),$$
$$a^k(4,1) = (2/3v^0)\left(-f^0_{4h}T^{0^{3/2}}(k_x^2 + k_y^2) + f^0_{2v}T^{0^{1/2}} - f^0_{5v}T^{0^{3/2}}\right),$$
$$a^k(4,2) = (2\mathrm{i}/3v^0)\left(-f^0_1 T^0 k_x + 2f^0_2 T^{0^{1/2}}k_y\right),$$
$$a^k(4,3) = (2\mathrm{i}/3v^0)\left(2f^0_2 T^{0^{1/2}}k_x - f^0_1 T^0 k_y\right),$$
$$a^k(4,4) = (2/3v^0)\left(-f^0_4(k_x^2 + k_y^2) - f^0_5\right)T^{0^{1/2}}.$$

Note that the subscripts σ and v indicate partial derivatives, and the superscript 0 denotes quantities evaluated at the base state.

Appendix B. Coefficients in the dispersion relation

The coefficients in the dispersion relation (4.5) are

$$a_3 = \left[\frac{2}{3v^0}h_3 + \frac{1}{v^0}\left(h_5 + f_2^0\right)k_{y0}^2\right] T^{0\,1/2}, \tag{B 1}$$

$$a_2 = \left[\frac{h_2}{T^0} + \tfrac{2}{3v^{0\,2}}\left(f_1^{0\,2} + \frac{f_2^{0\,2}}{T^0} + h_3h_5 + f_2^0\left(h_3 + \tfrac{3}{2}h_5k_{y0}^2\right)\right)\right] T^0k_{y0}^2, \tag{B 2}$$

$$a_1 = \frac{2}{3v^0}\left[\frac{1}{v^{0\,2}}f_2^0h_5\left(h_3 + f_5^0\right)k_{y0}^2 + \frac{1}{v^{0\,2}}f_1^0f_2^0\left(f_1^0k_{y0}^2 + \frac{2v^0}{T^0}\right) + f_1^0h_4 + \frac{h_2}{T^0}\left(h_3 + \tfrac{3}{2}f_2^0k_{y0}^2\right)\right] T^{0\,3/2}k_{y0}^2, \tag{B 3}$$

$$a_0 = \frac{2}{3v^{0\,2}}\left[\frac{h_2}{T^0}\left(h_3 + f_5^0\right) + \left(h_4 - \frac{2h_1}{T^{0\,3/2}}\right)f_1^0\right] f_2^0\,T^{0\,2}k_{y0}^4, \tag{B 4}$$

where

$$h_1 = \left(f_{2v}^0\,T^{0\,1/2} + \tau_v^0\right) > 0, \tag{B 5}$$

$$h_2 = \left(f_{1v}^0\,T^0 + \sigma_{cv}^0\right) > 0, \tag{B 6}$$

$$h_3 = \left(f_4^0k_{y0}^2 + f_5^0\right) > 0, \tag{B 7}$$

$$h_4 = -\left(f_{4h}^0k_{y0}^2 - \left(f_{2v}^0/T^0\right) + f_{5v}^0\right) \leqslant 0, \tag{B 8}$$

$$h_5 = \left(f_3^0 + \tfrac{4}{3}f_2^0\right) + \frac{1}{T^{0\,1/2}}\left(\tau^0 - \frac{1}{\tau_{\sigma\sigma}^0}\right) > 0. \tag{B 9}$$

The dispersion relation for the incompressible case is given by

$$\omega^2 + a_1\omega + a_0 = 0, \tag{B 10}$$

where

$$a_1 = \frac{1}{v^0}\left[\left(f_2^0 + \tfrac{2}{3}f_4^0\right)k_{y0}^2 + \tfrac{2}{3}f_5^0\right] T^{0\,1/2} > 0, \tag{B 11}$$

$$a_0 = \frac{2}{3v^{0\,2}}f_2^0k_{y0}^2\left[\left(f_4^0k_{y0}^2 + f_5^0\right)T^0 + f_2^0\right] > 0. \tag{B 12}$$

Appendix C. Multiplicative integral method

We consider the following matrix differential equation:

$$\frac{\mathrm{d}\boldsymbol{Y}}{\mathrm{d}t} = \boldsymbol{A}(t)\boldsymbol{Y}, \quad \boldsymbol{Y}(0) = \boldsymbol{I} \tag{C 1}$$

where $\boldsymbol{A}(t)$ is a continuous matrix function of the argument t in some arbitrary (finite/infinite) interval (a, b).

The normalized solution of (C1), often called the matricant, can be represented in

the form of an infinite series (Gantmacher 1960)

$$\boldsymbol{Y}(t) = \boldsymbol{\Pi}_{t_0}^{t} = \boldsymbol{I} + \int_{t_0}^{t} \boldsymbol{A}(\chi)\mathrm{d}\chi + \int_{t_0}^{t} \boldsymbol{A}(\chi) \int_{t_0}^{\chi} \boldsymbol{A}(\xi)\mathrm{d}\xi\mathrm{d}\chi + \cdots. \tag{C 2}$$

It can be shown that the matricant converges absolutely and uniformly in every closed interval in which $\boldsymbol{A}(t)$ is continuous. The matricant satisfies a well-known property:

$$\boldsymbol{\Pi}_{t_0}^{t} = \boldsymbol{\Pi}_{t_1}^{t}\, \boldsymbol{\Pi}_{t_0}^{t_1} \quad \forall \quad (t_0, t_1, t) \in (a, b). \tag{C 3}$$

To compute the matricant, we divide the time interval (t_0, t) into m parts by introducing points $t_1, t_2, \ldots, t_{m-1}$ and set $\Delta t_k = t_k - t_{k-1}$, $k = 1, 2, \ldots, m$ with $t_m = t$. By the property of the matricant (C3) we write

$$\boldsymbol{\Pi}_{t_0}^{t} = \boldsymbol{\Pi}_{t_{m-1}}^{t} \ldots \boldsymbol{\Pi}_{t_1}^{t_2} \boldsymbol{\Pi}_{t_0}^{t_1}. \tag{C 4}$$

Considering Δt_k as small quantities of first order we can compute $\boldsymbol{\Pi}_{t_{k-1}}^{t_k}$ to within an error of $O(\Delta t_k^2)$ as

$$\boldsymbol{\Pi}_{t_{k-1}}^{t_k} = \boldsymbol{I} + \int_{t_k}^{t_{k-1}} \boldsymbol{A}(\chi)\mathrm{d}\chi + \text{h.o.t.} \tag{C 5}$$

Combining (C4) and (C5) we obtain

$$\boldsymbol{\Pi}_{t_0}^{t} \cong \left[\boldsymbol{I} + \int_{t_{n-1}}^{t} \boldsymbol{A}(\chi)\mathrm{d}\chi\right] \ldots \left[\boldsymbol{I} + \int_{t_1}^{t_2} \boldsymbol{A}(\chi)\mathrm{d}\chi\right] \left[\boldsymbol{I} + \int_{t_0}^{t_1} \boldsymbol{A}(\chi)\mathrm{d}\chi\right]. \tag{C 6}$$

By decreasing the size of the time interval Δt the error can be brought down and thus we obtain the exact limit formula:

$$\boldsymbol{\Pi}_{t_0}^{t} = \lim_{\Delta t_k \to 0} \left[\boldsymbol{I} + \int_{t_{n-1}}^{t} \boldsymbol{A}(\chi)\mathrm{d}\chi\right] \ldots \left[\boldsymbol{I} + \int_{t_1}^{t_2} \boldsymbol{A}(\chi)\mathrm{d}\chi\right] \left[\boldsymbol{I} + \int_{t_0}^{t_1} \boldsymbol{A}(\chi)\mathrm{d}\chi\right]. \tag{C 7}$$

This gives a representation of the matricant in the form of a multiplicative integral.

REFERENCES

Alam, M. 1997 Stability of unbounded and bounded granular shear flows. PhD thesis (in preparation), Indian Institute of Science, Bangalore.

Atkinson, J. H. & Bransby, P. L. 1982 *The Mechanics of Soils*. McGraw-Hill.

Babić, M. 1993 On the stability of rapid granular flows. *J. Fluid Mech.* **254**, 127–150.

Behringer, R. P. & Baxter, G. W. 1991 Pattern formation and complexity in granular flows. In *Granular Matter: An Interdisciplinary Approach* (ed. A. Mehta), pp. 85–119. Springer.

Bender, C. M. & Orszag, S. A. 1984 *Advanced Mathematical Methods for Scientists and Engineers*. McGraw-Hill.

Butler, K. M. & Farrell, B. F. 1992 Three-dimensional optimal perturbations in viscous shear flow. *Phys. Fluids* A **4**, 1637–1650.

Butler, K. M. & Farrell, B. F. 1994 Nonlinear equilibration of two-dimensional optimal perturbations in viscous shear flow. *Phys. Fluids* A **6**, 2011–2020.

Drazin, P. G. & Reid, W. H. 1981 *Hydrodynamic Stability*. Cambridge University Press.

Gantmacher, F. R. 1960 *Matrix Theory*, Vol. II. Chelsea.

Goldhirsch, I., Tan, M-L. & Zanetti, G 1993 A molecular dynamical study of granular fluids **I**: the unforced granular gas in two dimensions. *J. Sci. Comput.* **8**, 1–40.

Hopkins, M. A. & Louge, M. Y. 1991 Inelastic microstructure in rapid granular flows of smooth disks. *Phys. Fluids* A **3**, 47–57.

Jackson, R. 1983 Some mathematical and physical aspects of continuum models for the motion of granular materials. In *Theory of Dispersed Multiphase Flow* (ed. R. Meyer), pp. 291–337. Academic.

Jackson, R. 1986 Some features of the flow of granular materials and aerated granular materials. *J. Rheol.* **30**, 907–930.

Jenkins, J. T. & Richman, M. W. 1985 Kinetic theory for plane shear flows of a dense gas of identical, rough, inelastic, circular disks. *Phys. Fluids* **28**, 3485–3494.

Johnson, P. C. & Jackson, R. 1987 Frictional-collisional constitutive relations for granular materials, with application to plane shearing. *J. Fluid Mech.* **176**, 67–93.

Johnson, P. C., Nott, P. R. & Jackson, R. 1990 Frictional-collisional equations of motion for particulate flows and their application to chutes. *J. Fluid Mech.* **210**, 501–536.

Jyotsna, R. 1993 Frictional-kinetic models for steady cohesionless granular flow through a wedge-shaped hopper. PhD thesis, Indian Institute of Science, Bangalore.

Landhal, M. T. 1980 A note on an algebraic instability of inviscid parallel shear flows. *J. Fluid Mech.* **98**, 243–251.

Lun, C. K., Savage, S. B., Jeffrey, D. J. & Chepurniy, N 1984 Kinetic theories for granular flow: inelastic particles in Couette flow and slightly inelastic particles in a general flow field. *J. Fluid Mech.* **140**, 223–256.

McNamara, S. 1993 Hydrodynamic modes of a uniform granular medium. *Phys. Fluids* A **5**, 3056–3070.

Mello, T. M., Diamond, P. H. & Levine, H. 1991 Hydrodynamic modes of a granular shear flow. *Phys. Fluids* A **3**, 2067–2075.

Miller, T. M., O'Hern, C. & Behringer, R. P. 1996 Stress fluctuations for continuously sheared granular materials. *Phys. Rev. Lett.* **77**, 3110–3113.

Moffatt, H. K. 1967 The interaction of turbulence with strong wind shear. In *Atmospheric Turbulence and Radio Wave Propagation* (ed. A. M. Yaglom & V. I. Tatarsky), pp. 135–156. Moscow: Nauka.

Nott, P. R. & Jackson, R. 1992 Frictional-collisional equations of motion for granular materials and their application to flow in aerated chutes. *J. Fluid Mech.* **241**, 125–144.

Prakash, J. R. & Rao, K. K. 1988 Steady compressible flow of cohesionless granular materials through a wedge-shaped hopper; the smooth wall, radial gravity problem. *Chem. Engng Sci.* **43**, 479–494.

Reddy, S. C. & Henningson, D. S. 1993 Energy growth in viscous channel flows. *J. Fluid Mech.* **252**, 209–238.

Reddy, S. C., Schmid, P. J. & Henningson, D. S. 1993 Pseudospectra of the Orr-Sommerfeld operator. *SIAM J. Appl. Maths* **53**, 15–45.

Savage, S. B. 1992*a* Numerical simulations of Couette flow of granular materials: spatio-temporal coherence and 1/f noise. In *Physics of Granular Media* (ed. D. Bideau & J. Dodds), pp. 343–362. New York: Nova Science.

Savage, S. B. 1992*b* Instability of unbounded uniform granular shear flow. *J. Fluid Mech.* **241**, 109–123.

Savage, S. B. & Sayed, M. 1984 Stresses developed by dry cohesionless granular materials sheared in an annular shear cell. *J. Fluid Mech.* **142**, 391–430.

Schmid, P. J. & Kytömaa, H. K. 1994 Transient and asymptotic stability of granular shear flow. *J. Fluid Mech.* **264**, 255–275.

Thomson, W. 1887 Stability of fluid motion: rectilinear motion of viscous fluid between two parallel plates. *Phil. Mag.* **24**, 188–196.

Trefethen, L. N., Trefethen, A. E., Reddy, S. C. & Driscoll, T. 1993 Hydrodynamic stability without eigenvalues. *Science* **261**, 578–584.

Wang, C.-H., Jackson, R. & Sundaresan, S. 1996 Stability of bounded rapid shear flows of a granular material. *J. Fluid Mech.* **308**, 31–62.